TÉCNICO LISBOA

Yaw Rate Control in Autonomous Electric Vehicles: A Steering-Based Approach

Diogo Gabriel da Silva Bento

Thesis to obtain the Master of Science Degree in

Electrical and Computer Engineering

Supervisors

Professor José António da Cruz Pinto Gaspar
Professor João Filipe Pereira Fernandes

Examination Committee

Chairperson: Professor António Manuel Raminhos Cordeiro Grilo
Supervisor: Professor José António da Cruz Pinto Gaspar
Member of the Committee: Professor Duarte Pedro Mata de Oliveira Valério

June 2024

Declaration

I declare that this document is an original work of my own authorship and that it fulfills all the requirements of the Code of Conduct and Good Practices of the Universidade de Lisboa.

Agradecimentos

Estando a chegar ao fim do meu percurso académico, quero aproveitar para agradecer aqui a algumas pessoas que fizeram parte desta jornada.

Primeiramente, quero dirigir um obrigado à minha mãe e ao meu pai, pelos sacrifícios feitos ao longo dos meus 24 anos de vida, que me permitiram aqui chegar.

De seguida, aos meus orientadores, professor João Fernandes e professor José Gaspar, por toda ajuda dada desde o início da tese.

Quero também agradecer especialmente à minha namorada Ana, por todas as noites que passou ao meu lado na biblioteca e por todo o apoio dado em qualquer coisa que precisasse.

E por fim, quero agradecer aos meus restantes familiares e amigos.

Resumo

A proliferação de veículos autónomos apresenta inúmeros desafios para os sistemas de controlo de veículos, especialmente para garantir normas de segurança que satisfaçam ou excedam as dos condutores humanos. Para uma adoção generalizada, os veículos autónomos têm de demonstrar segurança e fiabilidade superiores. Historicamente, a segurança dos veículos melhorou significativamente com a introdução de novas tecnologias como os cintos de segurança, os sistemas de travagem anti-bloqueio (ABS) e o controlo eletrónico de estabilidade (ESC), tecnologias que comprovadamente salvam vidas.

Esta tese propõe um novo controlador de yaw-rate que controla a direção, para melhorar a segurança do veículo. Este controlador centra-se no sistema de direção, um dos componentes críticos do veículo. Os avanços nos veículos autónomos e a implementação da tecnologia steer-by-wire permitiram o desenvolvimento desta abordagem de controlo inovadora.

Foram realizadas experiências em simulação, no âmbito do projecto VIENA, para avaliar o desempenho do controlador de yaw-rate proposto. Estas simulações utilizaram o teste do alce para testar a eficácia do controlador na manutenção da estabilidade do veículo e na aderência à trajetória desejada. Os resultados obtidos a partir destas simulações são promissores, indicando melhorias significativas na estabilidade e no controlo do veículo em comparação com os sistemas anteriormente utilizados.

As conclusões sugerem que o controlador proposto tem potencial para aumentar a segurança dos veículos. Isto sublinha a importância da inovação contínua nos sistemas de controlo para garantir o funcionamento seguro e fiável dos veículos autónomos, abrindo caminho para a sua maior aceitação e integração na vida quotidiana.

Palavras chave: Controlador eletrónico de estabilidade, Controlador de yaw-rate, Veículo autónomo, Veículo Elétrico, Teste do Alce, Steer-by-wire.

Abstract

The rise of autonomous vehicles presents numerous challenges for vehicle control systems, particularly in ensuring safety standards that meet or exceed those of human drivers. For widespread adoption, autonomous vehicles must demonstrate superior safety and reliability. Historically, vehicle safety has significantly improved with the introduction of technologies such as seatbelts, anti-lock braking systems (ABS) and electronic stability control (ESC), all of which are now standard and have been proven to save lives.

This thesis proposes a novel controller aimed at further enhancing vehicle safety: a steering-based yaw rate controller. This controller focuses on the steering system, a critical component responsible for guiding the vehicle along its desired trajectory. The advancements in autonomous vehicles and the implementation of steer-by-wire technology have enabled the development of this innovative control approach.

Extensive simulation experiments were conducted to evaluate the performance of the proposed steering-based yaw rate controller as part of the VIENA project. These simulations utilized the standardized double lane-change manoeuvre to test the controller's effectiveness in maintaining vehicle stability and adhering to the desired path. The results obtained from these simulations are promising, indicating significant improvements in vehicle stability and control compared to previously used systems.

The findings suggest that the proposed controller has the potential to enhance the safety of vehicles. This research underscores the importance of continuous innovation in control systems to ensure the safe and reliable operation of autonomous vehicles, paving the way for their broader acceptance and integration into everyday life.

Keywords: Electronic Stability Controller, Yaw Rate Controller, Autonomous Vehicle, Electric Vehicle, Moose Test, Steer-by-wire.

Contents

List of Figures

List of Tables

List of Acronyms

3DOF	Three Degrees Of Freedom
ABS	Anti-lock Braking System
AEB	Automated Emergency Braking
CG	Center of Gravity
ECU	Electronic Control Unit
ESC	Electronic Stability Control
FOC	Field Oriented Control
IMU	Inertial Measurement Unit
ISO	International Organization for Standardization
IST	Instituto Superior Técnico
MIMO	Multiple Input Multiple Output
MPC	Model Predictive Control
PID	Proportional-Integral-Derivative
PCHIP	Piecewise Cubic Hermite Interpolating Polynomial
SISO	Single Input Single Output
VIENA	Intelligent Electric Vehicle with Autonomous Navigation
WHO	World Health Organization

Chapter 1

Introduction

Vehicles are becoming increasingly more automated, from already established technologies such as cruise control, lane keeping assistance and autonomous emergency braking (AEB), to future completely autonomous vehicles [19]. It is clear that in the future, autonomous vehicles will have several widespread applications, such as, performing taxi like services, delivering of goods, on privately owned vehicles and will be used on a daily basis [5]. It is left to us, engineers and researchers, to bridge the gap in terms of technological advancements necessary, to make autonomous vehicles a reality.

Autonomous vehicles have the potential to increase vehicle safety, since most of the car crashes are related to human distraction, intoxication or tiredness [10]. However, this transfers the responsibility to the people that project them and the safety systems that are put in place. Taking this into consideration, this thesis proposes the implementation of an Electronic Stability Controller (ESC) on an autonomous electric vehicle that will be used pedagogically. This autonomous electric vehicle is called VIENA project.

The main purpose of an ESC is to improve vehicle stability, by correcting understeer and oversteer behaviours, while cornering. It achieves this by applying the brakes in specific wheels when it detects a loss of traction, also known as skidding. However, a novel approach will be proposed, focusing on a steering-based yaw rate controller.

1.1 Related Work

There are several thesis already done about VIENA project, each one of them contributing to the development and improvement of this project. Starting with Filipe Parrado's thesis [20], passing through João Vargas' [28] and Fábio Portelinha's[21], and now the last ones

from Francisco Enguita [6] and João Fino [8]. This last one will be more influential in this thesis project, being presented more in-depth in Section 3.2. In those previously mentioned thesis were developed the steering controller, the speed profiler and the model predictive controller (MPC) [33] [26], these subsystems are now essential parts of VIENA.

1.2 Problem Formulation

Vehicles do not behave like the kinematic models in the real world, unless they are traveling at a low speed. Considering this, how can we develop controllers that perform well in the real world, where a car is traveling at higher speeds?

Considering dynamic models, involving forces in action on the real vehicle, allows simulating skid, rollover, understeer, oversteer, locked wheels, etc. Simulations allow assessing the limitations of the Model Predictive Controller (MPC) proposed in previous dissertations.

Given that we have a simulated vehicle that behaves more realistically, the need arises to correct the mentioned undesirable behaviours, in order to increase vehicle safety. In this thesis, we propose preventing and correcting understeer and oversteer, through the integration of a steering-based Electronic Stability Controller in series with the previously available MPC.

1.3 Report Structure

Chapter 1 introduces the problem to approach in the thesis, in particular, presents a short discussion on the state of the art on autonomous vehicles and on how to develop realistic models. Chapter 2 presents an overview of cornering vehicle dynamics and the state of the art on Electronic Stability Controllers (ESC) and Anti-lock Braking Systems (ABS). Chapter 3 presents VIENA's project background, describes the integration of an ESC with VIENA and outlines the proposed block diagram for this thesis. Chapter 4 provides an overview of the yaw rate controller and how it will be implemented in this thesis. Chapter 5 provides an overview of the different experiments executed as well as the results attained. Chapter 6 summarizes the work performed and presents a discussion on the advantages brought up by the chosen controller.

Chapter 2

Background and State of the Art

Intelligent Electric Vehicle with Autonomous Navigation (VIENA), is a project based on a Fiat Seicento Elettra, a production electric vehicle. The original car had a 30 [kW] asynchronous electric motor and was powered by a 12 [V] lead-acid battery system, but had no autonomous capabilities. The objective of this project is to convert the Fiat Seicento Elettra into an autonomous vehicle, so it can be used as a learning platform for IST students and as a Research and Development platform.

2.1 Vehicle Dynamics

In this Section we will take a look into some expressions and figures, which help to understand what happens to a vehicle while cornering. We will start with the equations that define the movement of a kinematic bicycle model and continue to expressions that contain the forces applied to a turning vehicle. By considering the forces applied we will be able to build a more accurate model of the vehicle.

Kinematic Single Track Model

In order to develop path-following controllers, previous theses started with a kinematic bicycle model and then proceeded more recently to a 3DOF dynamic model available in MATLAB/Simulink, see Section 3.2. Therefore, to have a better understanding of the previous work done, it will be presented a brief overview of the kinematic bicycle model with its basic equations [19]. The kinematic bicycle model is one of the easiest ways of implementing a vehicle model, since it only needs four equations to be defined.

In Figure 2.1 it is represented the kinematic single track model. This model consists

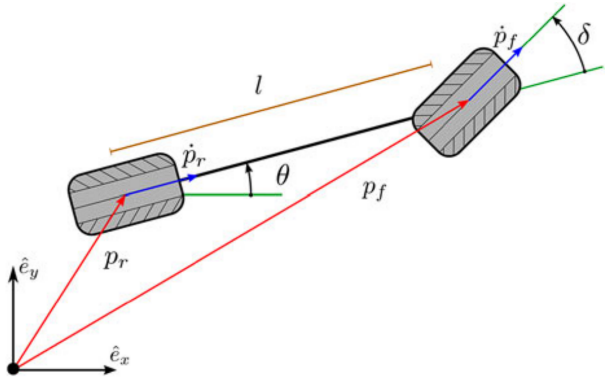

Figure 2.1: Kinematics of the single track model. From [19].

of two wheels connected by a rigid link, the front wheel is capable of rotating, in order to model steering. Wheel slip is not considered in this model. The model is defined by

$$\begin{cases} \dot{x}_f = v_f cos(\theta + \delta) \\ \dot{y}_f = v_f sin(\theta + \delta) \\ \dot{\theta} = \dfrac{v_f}{l} sin(\delta) \\ \dot{\delta} = v_\delta \end{cases} \tag{2.1}$$

where x_f and y_f are the front wheel coodinates, v_f is the front wheel speed, θ the steering angle, δ the vehicle heading, l the wheel base and v_δ is the steering rate. These equations define the kinematic model and provide a simple way of implementing it.

Steady-State Cornering

In this Section we will follow a base reference book [9] to introduce concepts necessary for the thesis, regarding cornering.

In Figure 2.2 it is represented the geometry of a turning vehicle. We can observe that the outer front wheel has a bigger corner radius than the inner front wheel. This results in the outer wheel needing a lower steering angle than the inner wheel, to keep the tires from slipping sideways. In order to give the right amount of steering angle to both wheels, the Ackerman steering geometry is used. There are also other steering geometries but for simplicity's sake they will not be considered.

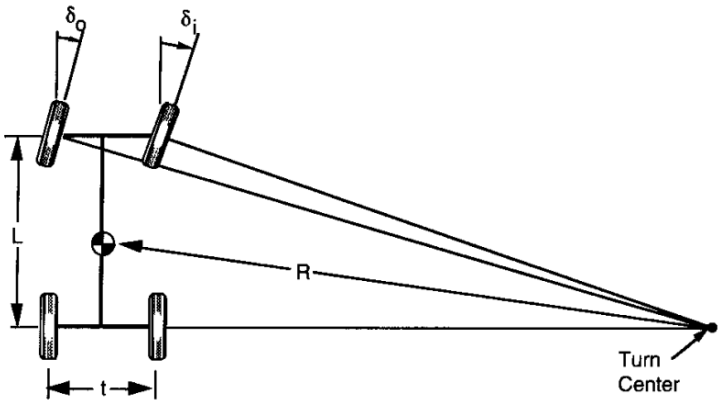

Figure 2.2: Geometry of a turning vehicle. From [9].

In the Ackerman steering geometry, an approximation of the steering angle given to each steerable wheel is given by,

$$\begin{cases} \delta_o \cong \dfrac{L}{R + t/2} \\ \delta_i \cong \dfrac{L}{R - t/2} \end{cases} . \tag{2.2}$$

Both angles are dependent on the vehicle track width t, distance between axles L (wheelbase) and corner radius R.

The Ackerman angle, which is the average angle of the front wheels, is given by a similar equation to the expressions above but without the track width,

$$\delta = \frac{L}{R} \quad . \tag{2.3}$$

As we can observe in Figure 2.3 for low values of slip angle, the relation between the lateral force F_y and the slip angle is linear, therefore, it can be given by

$$F_y = C_\alpha \alpha, \tag{2.4}$$

where C_α is denoted as the cornering stiffness, and α is the slip angle.

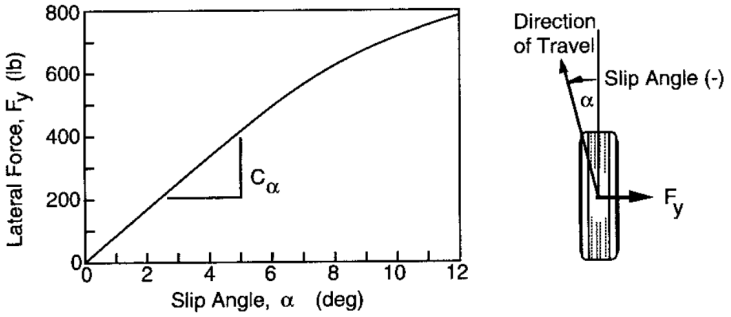

Figure 2.3: Tire cornering force properties. From [9].

Considering a vehicle doing a corner of radius R with speed V, the centripetal acceleration is given by

$$a_c = \frac{V^2}{R} \quad . \tag{2.5}$$

By applying Newton's second Law to the steady state corner the following equation is obtained

$$\sum F_y = ma_c \quad , \tag{2.6}$$

where m is the vehicle's mass. Therefore, substituting 2.5 in 2.6 and expanding the lateral forces, the cornering forces are given by

$$\sum F_y = F_{yf} + F_{yr} = F_{yfl} + F_{yfr} + F_{yrl} + F_{yrr} = m\,\frac{V^2}{R} \quad , \tag{2.7}$$

where F_{yf} and F_{yr} are the lateral tire forces in the front and rear axles, respectively. F_{yfl}, F_{yfr}, F_{yrl} and F_{yrr} are the lateral forces in the front-left, front-right, rear-left and rear-right tires, respectively.

Skidding and Rollover

In this Section we will follow the paper [29] to introduce the cornering limits to avoid skidding and rollover.

Assuming that the vehicle travels with a speed v_n and a longitudinal acceleration a_n, in a perfect circle of radius v_n/ω_n, we can observe in Figure 2.4 the relevant forces applied to the vehicle.

In order to avoid skidding while cornering, the normal force $F^{\perp}$ multiplied by the friction coefficient should be higher than the horizontal force on the tires F_h. Therefore,

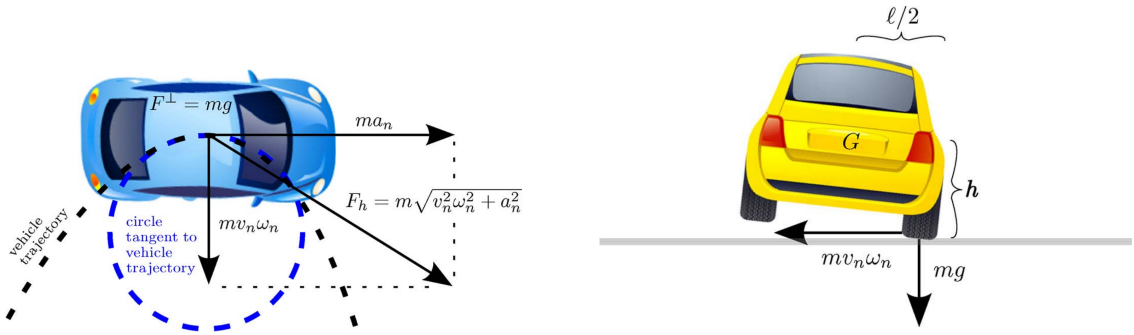

(a) Skid avoidance (b) Roll avoidance

Figure 2.4: Skid and rollover avoidance. From [29].

the following expression should be verified

$$F^{\perp}\mu > F_h <=> mg\mu > m\sqrt{v_n^2\omega_n^2 + a_n^2}, \tag{2.8}$$

where g is the gravitational acceleration and μ the coefficient of friction. The expression can be simplified to

$$\mu > \frac{1}{g}\sqrt{v_n^2\omega_n^2 + a_n^2}. \tag{2.9}$$

From this we can conclude that increasing the tire coefficient, will increase resistance to skidding, which is expected [24].

In order to avoid a rollover event, the torque $mgl/2$ created by the gravity force should be higher than the torque $mv_n\omega_n h$ created by the centripetal force, then following expression should be verified

$$mgl/2 > mv_n\omega_n h <=> gl/2 > v_n\omega_n h. \tag{2.10}$$

Which means that the resistance to rollover is highly dependant on the intrinsic characteristics of the vehicle, such as height of the center of gravity and track width. A bigger track width and a lower center of gravity positively influences rollover resistance.

2.2 Electronic Stability Control

The Electronic Stability Control (ESC) is an important technology, that improves the safety of cars, by improving the vehicle's behaviour while cornering and while performing evasive manoeuvres. This technology actuates the brakes in specific wheels in order to

correct under and oversteer behaviours, and to prevent rollovers. According to [7] the ESC helps to reduce fatalities by about 30% to 50% when comparing to vehicles not equipped with this technology, these numbers will be analysed in further detail in the Section regarding legislation and crash reduction.

Understeer/Oversteer

While cornering a vehicle can have two abnormal steering behaviours, it can be understeering or oversteering. It is considered as understeering when the vehicle turns less than the desired amount. This is the result of the front wheels not having traction enough to steer the car. It is considered as oversteering when the opposite occurs, when the vehicle turns more than the desired amount. This is the result of the rear wheels not having enough traction, to provide the reaction force necessary to counter the moment that makes the car rotate too much. These two behaviours are illustrated in Figure 2.5.

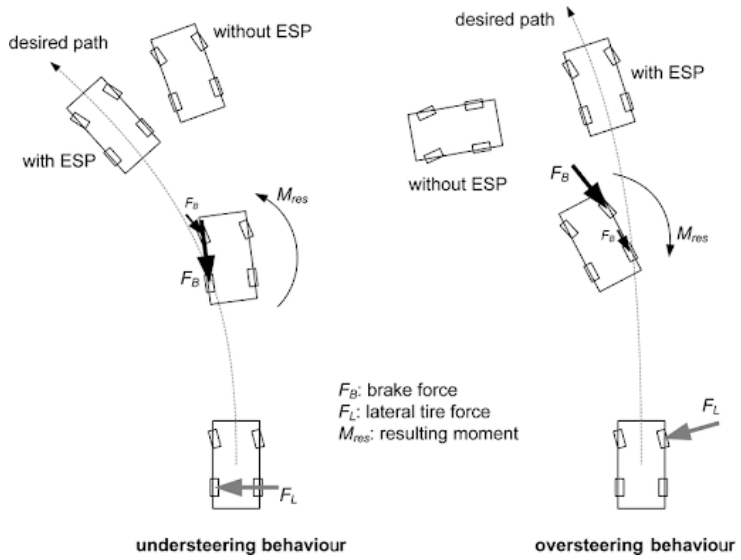

Figure 2.5: A Compensated-Yaw-Moment-Based Vehicle Stability Controller. From [4].

In order to correct these behaviours the ESC applies the brakes as illustrated by F_B in the aforementioned figure. To correct understeering, the brakes should be applied in the inner rear wheel, creating a moment that helps the car to rotate more. To correct oversteering, the brakes should be applied in the outer front wheel, to create a torque that counters the rotation. Both moments created are also illustrated in Figure 2.5.

A common solution is to use ABS hardware, sensors and actuators, to correct understeering/oversteering. A possible alternative solution, still to assess as literature review,

may be using motor acceleration or braking together with steering and counter-steering. To the best of our knowledge, this is not a solution yet used in cars, due to the lack of steer-by-wire systems. In today's vehicles using a motor to actuate the steering wheel, would rotate both the wheels and the steering wheel, since they are mechanically connected.

Moose Test/Double Lane Change manoeuvre

The Moose Test, also known as Double Lane Change Manoeuvre, was created to test the vehicle's performance while avoiding an obstacle. As the name indicates it simulates the situations where the car needs to avoid a moose that appears in the road. Besides the original intention of the test, it is very useful to evaluate the reaction of the vehicle when any unexpected obstacle appears in the road, being it an animal, a person, or even another car.

The Moose Test is illustrated in Figure 2.6, it consists in quickly changing lanes in order to avoid the cones and then coming back to the original lane. The test is performed at increasing speeds, until the car fails by knocking down the cones. This can be applied in a simulated environment in order to test the vehicle controller and the ESC.

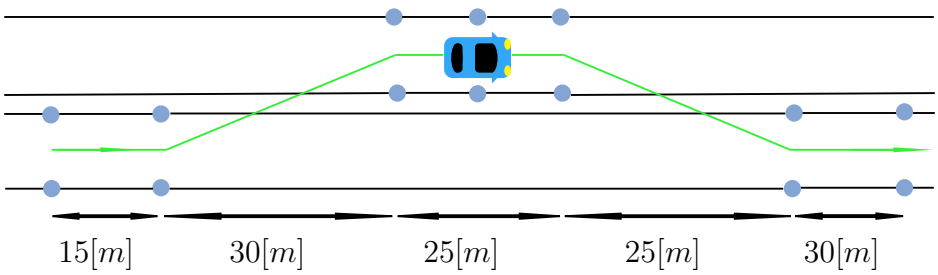

Figure 2.6: Double lane change manoeuvre. ISO 3888-1 [1].

Legislation and crash reduction

The ESC was first introduced in the 1990s in some vehicles, however, it was limited to very few models. As the efficacy of the ESC in avoiding fatalities was proven by several studies, some countries ended up making it mandatory for all new cars in the previous decade (2010s) [7]. The European Union made ESC mandatory for all new cars sold since 2014 and the United States of America made it mandatory since 2012.

In [7] is noted *The overwhelming majority of studies find that ESC is highly effective in reducing single-vehicle crashes in cars and SUVs. Fatal single-vehicle crashes involving*

cars are reduced by about $30-50\%$ *and SUVs by* $50-70\%$*. Fatal rollover crashes are estimated to be about* $70-90\%$ *lower with ESC regardless of vehicle type.*

In this thesis we propose studying and testing ESC in order to improve autonomous vehicles' safety systems. Increasing safety on road vehicles is extremely important, since according to the World Health Organization (WHO) there are anually 1.35 million fatalities on roadways [31].

2.3 Sensors, Actuators, Lock-ups and ABS

In order to implement the ESC is needed an IMU, that measures the yaw rate and lateral acceleration, a wheel speed sensor in each wheel and individual brake actuation for each wheel. Usually the ESC is implemented using the car's ABS since it already has the wheel speed sensors and a way to actuate the brakes. The ABS components will be presented in more detail in this Section.

Wheel Lock-ups

In Figure 2.7 it is represented the vehicle behaviour while braking, in case of a lock-up in the front tires and in the rear tires. With F_y being a disturbance force, M_s the disturbance torque and F_{yW} the reaction force from the wheel that still has traction. The lock-up was represented by marking the tire red.

In case of a wheel lock-up in the front tires the vehicle remains stable, due to being able to compensate the disturbance torque, through a reaction force from the rear wheels. But since the traction is reduced in the front tires, the vehicle cannot provide a steering force, so the vehicle becomes unsteerable. It goes straight independently of the input of the steering-wheel.

In the case of lock-up in the rear tires the vehicle becomes unstable, due to not being able to provide a reaction force to compensate the disturbance torque created. However, since the front tires still have traction, the vehicle is still steerable, but it will tend to spin due to the instability. From this behaviours we conclude that the front axle should lock-up before the rear one. The ABS is supposed to actuate before any lock-up occurs, in order to keep the vehicle stable and steerable while having a high deceleration.

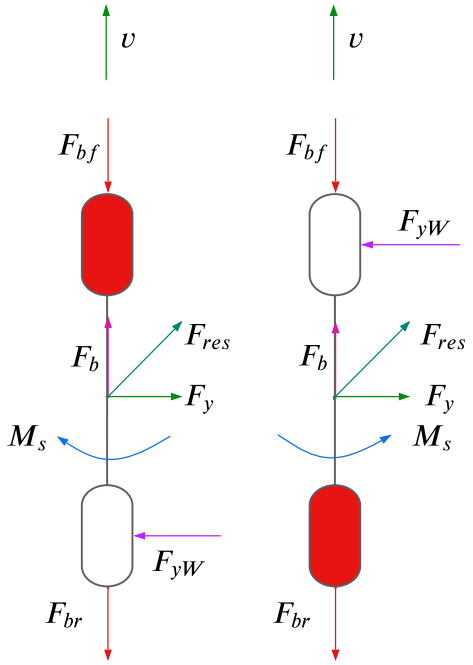

Figure 2.7: Front axle lock-up on the left and rear axle lock-up on the right.

Anti-lock Braking System (ABS)

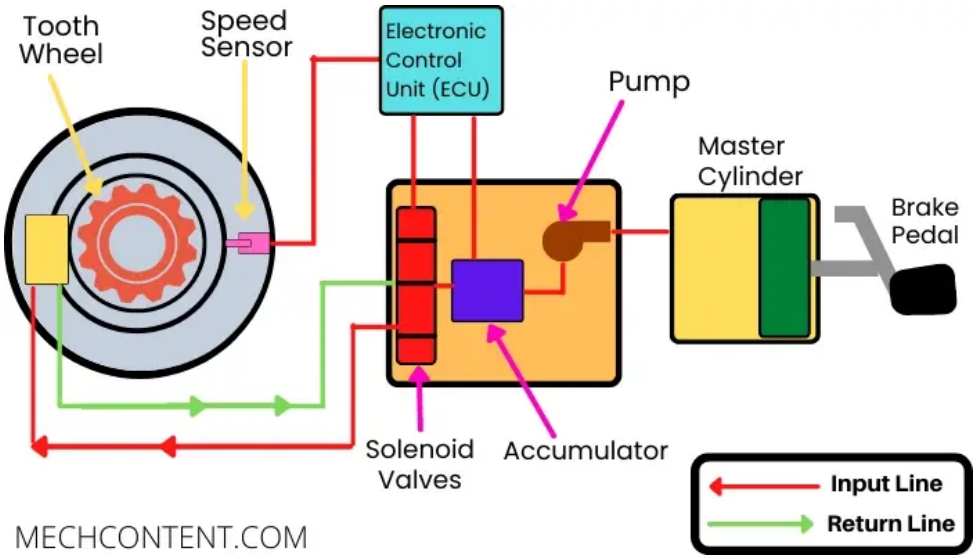

Figure 2.8: ABS diagram. From [22].

The anti-lock braking system (ABS) is a technology used in vehicles such as cars, trucks and airplanes, in order to improve their braking performance by preventing wheel lock-ups

and taking advantage of each individual wheel maximum grip available, at each instant. Resulting in a deceleration very close to the theoretical limit every time the brakes are fully pressed. The ABS also allows to keep the vehicle steerable and stable while braking, which would not occur in case of a wheel lock-up.

ABS systems in cars generally fall into two categories: a four-channel system, which employs wheel speed sensors and actuators in each wheel, and a three-channel system, where individual wheel speed sensors and actuation are present in the front wheels, while the rear wheel brakes are actuated with the same pressure.

Figure 2.8 depicts the components of the ABS system using a single-wheel representation. The ABS comprises a wheel speed sensor, brake hydraulic actuation, and an ECU. The hydraulic actuation includes a pump and a series of valves to adjust brake pressure as required.

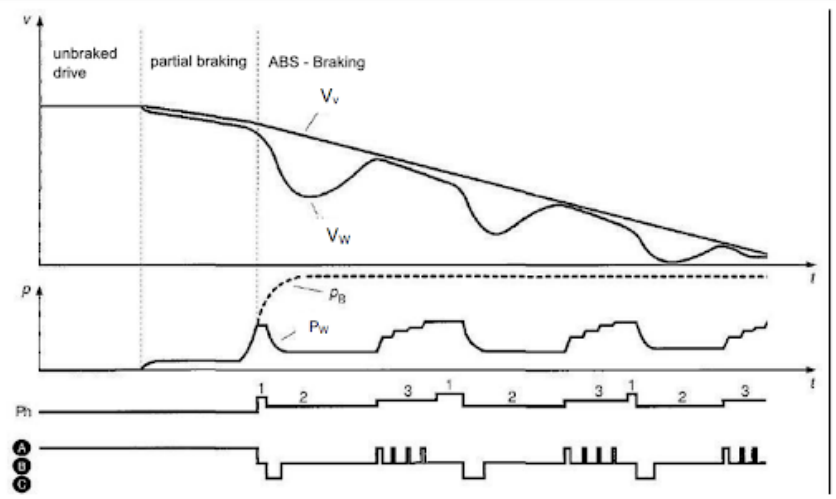

Figure 2.9: ABS Control cycle. From [3].

Figure 2.9 illustrates the brake line pressure, wheel speed and vehicle speed while hard braking. In the partial braking phase the wheel speed is just barely slower than the vehicle speed, so there is no action needed from the ABS. When the brake pressure is increased it results, in this case, in a fast deceleration of the wheel, which differs substantially from the vehicle's speed. This means that the wheel is about to lock-up, so the ABS system detects this and acts by decreasing the brake pressure through the brief opening of the outlet valve. The wheel speed increases again until it is close to the vehicle's speed. At

this point the inlet valve opens again, in order to increase the brake pressure. Then the process repeats until the vehicle comes to a stop.

This raises a question: How does the ABS system know that the vehicle is stopped, in order to not release the brakes? By the way the ABS works, it does not let the wheels stop completely, it should reduce the pressure and let them pick-up the speed again before that happens. Therefore, when the wheel speed sensors read that every wheel speed is zero or close to that, it will not release the pressure.

2.4 Steer-by-wire

Steer-by-wire is a technology that has been used on airplanes for many years and is now being applied in production vehicles.

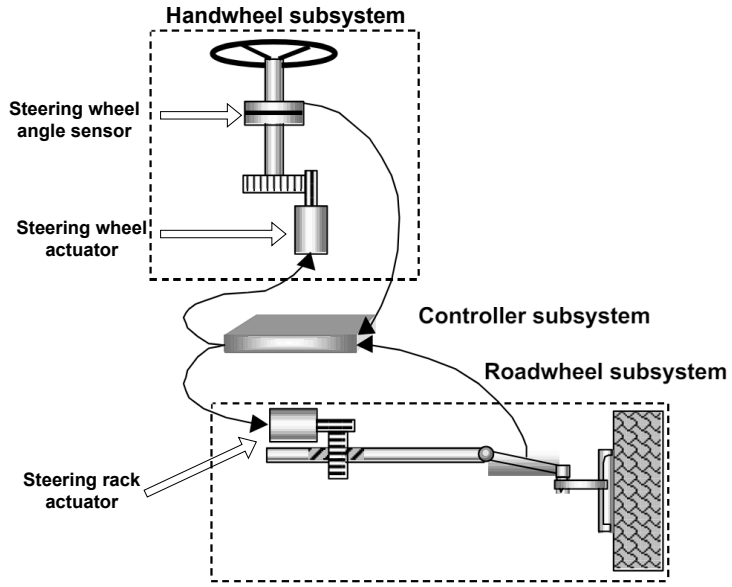

Figure 2.10: Steer-by-wire components. Modified from [11].

We can observe the main components of the system in Figure 2.10. It is composed by a steering wheel actuator, a steering wheel angle sensor, a steering rack actuator, and a controller. The steering rack actuator is responsible for the transmission of force feedback to the driver. This allows the driver to feel the road and gather information regarding the grip available at any moment. The steering wheel angle sensor registers the intended wheel angle input from the driver and sends that information to the controller. The steering rack actuator is responsible of steering the wheels. The controller uses the information given by the sensors to generate an output signal for the actuators. Some

brands like Lexus have redundant components, like two steering wheel actuators to ensure system safety.

As the wheel steering actuation is made using a controller, it is possible to change the sensitivity dependant on the vehicle speed. This allows for a steering wheel with a smaller lock-to-lock angle, this way the driver does not need to take the hands out of the steering wheel while performing difficult manoeuvres, like three point turns and parking. The controller is capable of increasing sensitivity at low speeds, to turn the wheels more with the same amount of steering wheel rotation and is capable of decreasing sensitivity at higher speeds to keep the vehicle stable, by turning the wheels less with the same steering wheel rotation.

Production vehicles have been using steer-by-wire since 2013, it was firstly introduced in the Infiniti Q50 [2]. However, this model had a hybrid steering system with steer-by-wire and a mechanical steering column. More recently pure steer-by-wire systems are starting to be used, with the already released Tesla Cybertruck [32] and the future release of Lexus RZ 450e [30], sometime this year.

The advent of steer-by-wire technology makes a steering-based yaw rate controller both useful and easier to implement. The yaw rate controller generates wheel angles, which can be sent to the steer-by-wire controller to maintain vehicle stability and ensure the vehicle stays on the desired trajectory.

Chapter 3

VIENA Electronic Stability Control

Figure 3.1: VIENA in the IST parking lot.

In this Chapter, the integration of an ESC with the VIENA project is discussed and developed. We consider simulated testing environments including skid, which are challenging for the MPC controller developed and tested in previous theses. The proposal for this thesis is to implement and integrate a steering-based ESC in series with the MPC.

We avoid trying to correct the MPC tuning because MPC uses a kinematic model rather than a dynamic one. This limitation means that, although MPC can be finely tuned for specific cases and speeds, it may fail in other situations due to its inability to account for the nonlinearities inherent in the system being controlled.

Simulation allows for the individual actuation of the four vehicle brakes and the measurement of each wheel's speed. However, VIENA (Figure 3.1) lacks an ABS system and will not have the capability to control the brakes individually. This limitation, combined

with the new steer-by-wire systems used in production vehicles, shifted the focus of this thesis to developing a controller that actuates the steering instead of the brakes. Such a controller can complement the various ESC systems implemented in today's vehicles.

Braking-based ESC systems have been extensively researched and used in production vehicles. Therefore, a steering-based controller will provide additional value. Additionally, we can leverage the already existing sensors in the vehicle, such as the steering angle sensor and the IMU, which measures lateral acceleration and yaw rate. This integration allows for the effective use of available data to enhance the vehicle's stability and control through the steering-based ESC system.

3.1 Complete System Model

In this thesis I will implement a steering-based ESC, between the controller and the VIENA car model blocks, in the diagram of Figure 3.2.

This VIENA block diagram is based on the work done by João Fino for his thesis [8]. He improved VIENA's model, previously it was being used a kinematic model and now it is being used a dynamic model. The dynamic model being used **Vehicle Body 3DOF** takes into account wheel slip, longitudinal and lateral acceleration, and yaw [14].

The controller architecture is composed by the Path Following Controller, the Electronic Stability Controller and the Vehicle Body 3DOF. The Path Following Controller receives as inputs the reference path coordinates $(\bar{x}, \bar{y})$, the reference speed $\bar{v_r}$ calculated by the speed profiler, the coordinates where the vehicle is positioned (x, y), vehicle speed v_r and vehicle yaw θ. The Path following controller then generates a steering angle δ that is sent to the ESC and the desired acceleration (a), that is sent directly to the Vehicle Body 3DOF.

The ESC takes as inputs the steering angle generated by the latter controller, the vehicle yaw rate γ and the vehicle speed v_r, and then generates a new steering angle δ' that will be the input of the Vehicle Body 3DOF. The Vehicle Body 3DOF simulates the vehicle with the mentioned inputs and reports the vehicle yaw rate, speed, position and yaw, based on the calculations made.

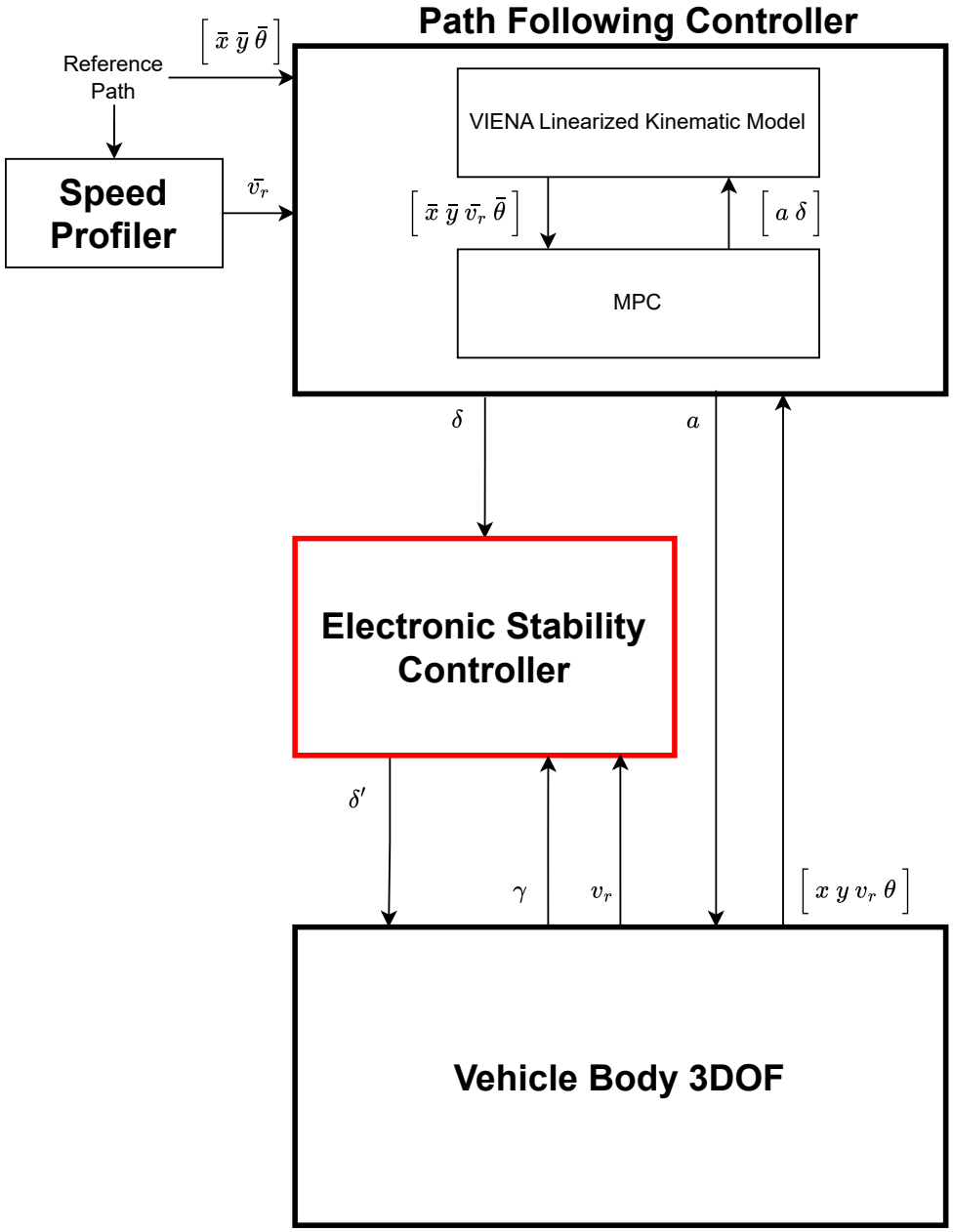

Figure 3.2: VIENA's Block Diagram, including the Electronic Stability Controller (ESC) to be introduced and developed in Section 3.4.

3.2 Vehicle Model

There are two Vehicle Body 3DOF models that can be used for the vehicle dynamics, a single-track and a dual-track model, Figure 3.3. João Fino [8] used the single-track model because the dual-track provides no advantages for his specific application, which is to

simulate slippage in corners at lower speeds. Additionally, the single-track model has a lower complexity.

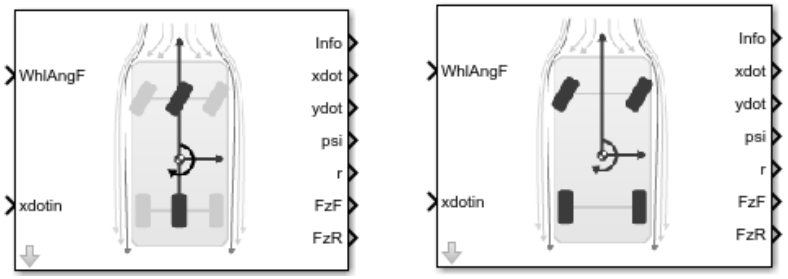

(a) Single Track (b) Dual Track

Figure 3.3: MATLAB's Vehicle Body 3DOF models. From [14].

However, the dual-track model was chosen for this thesis. In this work, it is relevant to consider the forces applied in each wheel, because at higher speeds the weight transfer plays a significant role,

$$\begin{cases} F_{zfo} = \dfrac{Mgl_r}{2L} + W_B + W_{TF} \\ F_{zfi} = \dfrac{Mgl_r}{2L} + W_B - W_{TF} \\ F_{zro} = \dfrac{Mgl_r}{2L} - W_B + W_{TR} \\ F_{zri} = \dfrac{Mgl_r}{2L} - W_B - W_{TR} \end{cases}, \tag{3.1}$$

where F_{zfo} is the vertical force in the outer front wheel, W_{TF} and W_{TR} the total front and rear weight transfers, respectively, W_B the longitudinal weight transfer resultant from braking, l_r the distance between the CG and the rear axle, and L the vehicle wheel-base [17].

The dual-track model, Figure 3.4 also provides a better platform for future projects, because it allows for the application of different brake forces for each individual wheel.

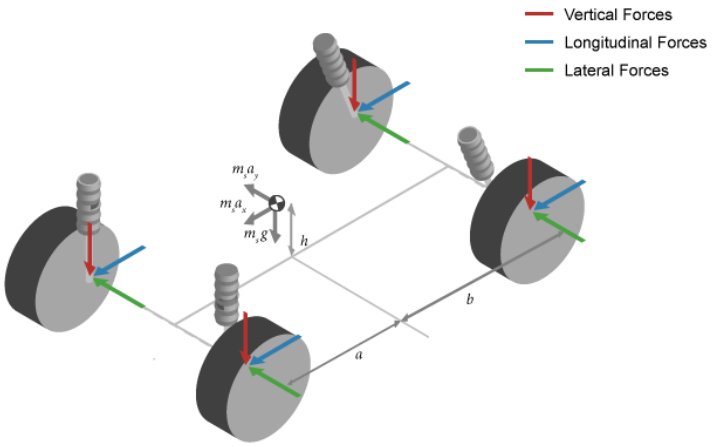

Figure 3.4: MATLAB's Vehicle Body 3DOF dual track model with the applied forces. From [14].

The dual-track model accepts as input, external longitudinal forces in each independent wheel, if in the model parameters the Axle forces are set to External longitudinal forces,

$$\begin{cases} F_{xflt} = F_{xflinput} \\ F_{xfrt} = F_{xfrinput} \\ F_{xrlt} = F_{xrlinput} \\ F_{xrrt} = F_{xrrinput} \end{cases}, \tag{3.2}$$

where F_{xflt}, F_{xfrt}, F_{xrlt} and F_{xrrt} are the longitudinal tire forces applied to the front left wheel, front right wheel, rear left wheel and rear right wheel, respectively. $F_{xflinput}$, $F_{xfrinput}$, $F_{xrlinput}$ and $F_{xrrinput}$ are the input longitudinal forces applied to the front left wheel, front right wheel, rear left wheel and rear right wheel, respectively. These external longitudinal forces can be used to model brake actuation.

The lateral forces are computed by the model itself using,

$$\begin{cases} F_{yflt} = -C_{yfl}\alpha_{fl}\mu_{fl}\dfrac{F_{zfl}}{2F_{znom}} \\ F_{yfrt} = -C_{yfr}\alpha_{fr}\mu_{fr}\dfrac{F_{zfr}}{2F_{znom}} \\ F_{yrlt} = -C_{yrl}\alpha_{rl}\mu_{rl}\dfrac{F_{zrl}}{2F_{znom}} \\ F_{yrrt} = -C_{yrr}\alpha_{rr}\mu_{rr}\dfrac{F_{zrr}}{2F_{znom}} \end{cases}, \tag{3.3}$$

where F_{yflt}, F_{yfrt}, F_{yrlt} and F_{yrrt} are the lateral tire forces applied to the front left wheel, front right wheel, rear left wheel and rear right wheel, respectively.

C_{yfl}, α_{fl}, μ_{fl}, F_{zfl} and F_{znom} are the front left wheel cornering stiffness, slip angle, friction coefficient, normal force applied on the vehicle-fixed z-axis and the sum of all nominal forces applied to the wheels on the vehicle fixed z-axis, respectively. The rest of the variables follow the same naming logic, only changing the wheel they refer to.

The 3DOF dual track model represents longitudinal, lateral and yaw motion, making it suitable to be used while cornering to detect and prevent skidding. However, the block does not take into account roll, pitch and elevation changes, making it unsuitable to design anti-rollover protection. Due to this limitation, there are two options to follow while designing the electronic stability controller. In the first option, it is assumed that skidding occurs before rollover would and, in this case, the Vehicle Body 3DOF is good enough.

In the second option, it is assumed that rollover can occur, due to the intrinsic characteristics of the vehicle, such as the height of the center of gravity and the car's track width. And in this case it is necessary to use a more complex model, such as Vehicle Body 6DOF, that model roll and pitch as well. All the heavy components like batteries and motor are placed in VIENA's floor, so we will assume that the vehicle has a low center of gravity and skidding will occur first. Thus, we will be using the 3DOF model instead of the 6DOF.

3.3 Double Lane-Change Manoeuvre Trajectory Generation

The Double Lane Change Manoeuvre is defined according to ISO 3888-1 [1] as the process of quickly changing the vehicle lane to a parallel one and then coming back to the original lane. The track layout can be seen in Figure 3.5. The test is considered to be completed successfully, if the vehicle completes the track without displacing any of the cones that represent the track limits.

The length of the track is constant at 125 [m], but the width of the different track Sections is dependant on the vehicle width and can be seen in Table 3.1. The track used in Chapter 5 follows the dimensions defined by the standard, using a vehicle width of 1.5 [m]. According to the calculations, the track width will range from 1.91 [m] in Section 1 to 2.21 [m] in Sections 5 and 6. In the narrowest part of the track, the vehicle will only

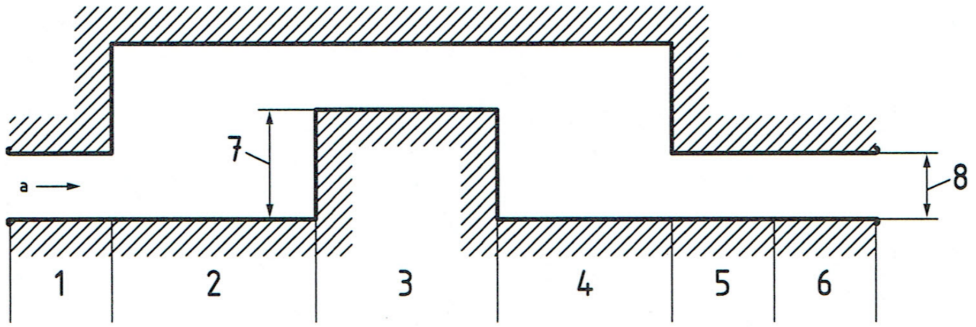

Figure 3.5: Double lane-change track, from [1]. The numbers 1 to 6 correspond to the Sections in Table 3.1, 7 is the lane offset, 8 is the track width and (a) is the driving direction.

have 20 [cm] of margin on each side, considering that it is centered in the lane. And on the widest part it will have 35 [cm] on each side.

Table 3.1: Double lane-change track dimensions defined in ISO 3888-1 [1]. These will be the dimensions used for the simulated track in Chapter 5.

Section	**Length [m]**	**(7) Lane offset [m]**	**(8) Width [m]**
1	15	-	1.1×vehicle width+0.25 = 1.91
2	30	-	-
3	25	3.5	1.2×vehicle width+0.25 = 2.06
4	25	-	-
5	15	-	1.3×vehicle width+0.25 = 2.21
6	15	-	1.3×vehicle width+0.25 = 2.21

In order to develop the simulated test track, I used the midpoints of the track limits from Sections 1, 3, 5 and 6. To connect the isolated trajectory points I made an interpolation using MATLAB's pchip (piecewise cubic hermite interpolating polynomial) function, documentation in [15]. Pchip interpolation generates a trajectory that passes through all given points and that is differentiable at any point. It also reduces overshoot and undershoot when comparing to a cubic interpolation [23]. The points were interpolated using an interval of 1 [m] in the x axis. This kind of interpolation was used due to being shape-preserving and generating a good trajectory so the vehicle is able to complete the track.

The track presented in this Section will be used in Chapter 5 to evaluate the performance of the yaw rate controller. The track will be used as a standardized test to compare the performance of the MPC alone and the yaw rate controller operating with the MPC.

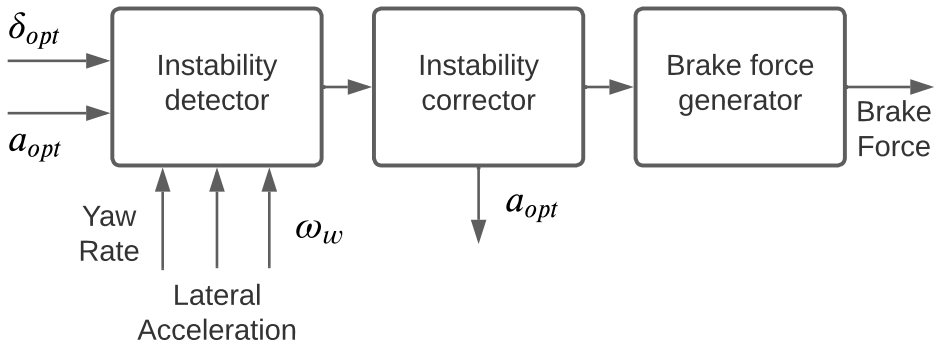

Figure 3.6: General ESC Block Diagram

3.4 Electronic Stability Control (ESC)

In Figure 3.6 there is an overview of a general Electronic Stability Controller (ESC), not the controller that is going to be proposed in this thesis. This is shown to better understand what a typical ESC looks like from the control perspective and how different it is from the proposed solution. The typical ESC is based in three main subsystems that will be detailed in the next paragraphs [34].

Input and output data An ESC system takes as inputs the steering angle, acceleration, yaw rate, the lateral acceleration and the individual wheel speed. The ESC would then return the individual wheel's braking forces to be applied and the desired motor acceleration. It is relevant that the ESC subsystem is able to change the motor's acceleration, since it is sometimes necessary to reduce or completely cutoff the torque transmitted from the motor to the wheels.

The first subsystem detects if the vehicle is understeering or oversteering and will send information about the situation to the next subsystem.

The second subsystem decides in which wheels, the brake force should be applied and if it should change the amount of acceleration of the car (this will reduce the motor torque if needed).

The third and last subsystem generates the brake force values, for each individual wheel, needed to correct the situation.

Yaw Rate The Electronic Stability Controller (ESC), as previously mentioned, comprises several systems. In this thesis, we focus on implementing one of the many capabilities of the ESC. Our primary interest is in improving stability while cornering, and to

address this, we propose a yaw rate controller.

Yaw rate control is a type of steering-based stability control. It is particularly relevant as modern vehicles increasingly adopt the necessary steer-by-wire technology (see Section 2.4). The yaw rate controller can be highly beneficial by overriding the driver's steering inputs and reacting much faster to unexpected road slippage conditions.

In this thesis, we propose the steering-based yaw rate controller for an autonomous vehicle. However, there is no reason it cannot also be applied to all human-driven vehicles equipped with steer-by-wire [25]. Details are provided in the next chapter.

Chapter 4

Yaw Rate Controller

In this Chapter, the yaw rate controller will be discussed in detail. We will begin by defining an error variable, based on the yaw rate, to feed into a control loop. The output of the controller will be the front wheel angles. The generated wheel angles are designed to maintain vehicle stability and ensure the vehicle stays on the desired trajectory.

Given a steering angle, one expects a certain curvature. However, wheels slippage may change the car motion, specifically its yaw rate. With an additional yaw rate estimation, in accordance with tires slippage, one may design a controller that mitigates that additional term.

The estimation of yaw rate error consists in comparing an observed yaw rate and an expected yaw rate, in order to generate a signal to be used as an input for the controller being developed. The expected yaw rate is an approximation of the yaw rate expected from a kinematic model for a given situation, with a term that accounts for the speed increase.

In order to test this controller concept with our model, some papers were used as a reference to obtain a formula that gives an expected yaw rate. To generate the control signal we will only need to subtract the observed yaw rate, given by MATLAB's 3DOF model, from the expected yaw rate.

Defining yaw rate error as expected yaw rate, minus observed yaw rate, yaw rate error is given by

$$e_\gamma = \gamma^* - \gamma \quad , \tag{4.1}$$

where γ^* is the expected yaw rate and γ is the observed yaw rate.

The expected yaw rate is given by

$$\gamma^* = \frac{1}{1 + AV^2} \frac{V}{l} \delta \quad , \tag{4.2}$$

where γ^* is the expected yaw rate, V the vehicle speed, l the distance between axles, δ the steering angle and A the stability factor [27]. The stability factor is then given by

$$A = -\frac{M}{2l^2} \frac{l_f C_f - l_r C_r}{C_f C_r} \quad , \tag{4.3}$$

where C_f is the front axis cornering stiffness, C_r the rear axis cornering stiffness, l_f the distance between the CG and the front axle, l_r the distance between the CG and the rear axle and M the vehicle mass. The stability factor is a concept introduced in [27] to take into consideration the speed increase, while calculating the expected yaw rate.

The implementation made in Simulink follows Figure 4.1 block diagram.

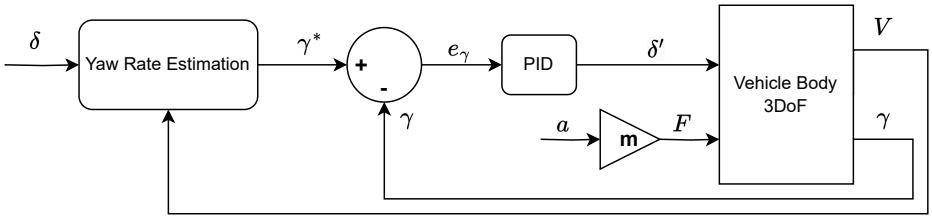

Figure 4.1: Block diagram implemented in Simulink.

This is the first prototype of a yaw rate controller using a simple PID controller for simplicity's sake. The input variables δ and a are given by the MPC controller that was implemented in previous thesis. The simplicity of this controller allowed for a faster implementation of a proof of concept. The controller follows a SISO architecture, although it should be improved and changed into a MIMO architecture, in order to take into account the different inputs available and the two control variables given to the Vehicle Body 3DoF model.

Inside the Yaw Rate Estimation, yaw rate estimate is computed according to (4.2).

4.1 Cornering Stiffness

Cornering stiffness, a parameter briefly introduced previously, which is given by (2.4), relates the tire slip angle and the force applied by the tire to the road [9]. It is an extremely important parameter while modeling a vehicle, since the tires are the only

interface between the vehicle and the road. Knowing the force applied by the tires allows the understanding and prediction of vehicle behaviour.

In order to simplify the model used initially, the cornering stiffness was assumed to be linear. However, this revealed to not be sufficient to model correctly the vehicle behaviour while skidding, since with the increase of the slip angle came an increase of the force applied.

This is a behaviour very different from what happens in the real world, since the force does not increase indefinitely with the slip angle, it reaches a limit and then starts to decrease. This made vehicle skidding not possible. In order to improve this behaviour, and to better model the limit of force a tire can apply to the road, a non linear cornering stiffness was introduced in the 3DOF vehicle body. This Simulink model allows the use of a mapped cornering stiffness and a relaxation index. The cornering stiffness used was mapped from [12]. The paper has four different curves for different vertical loads, so it was chosen the curve which is closer to our vehicle mass.

The mapped cornering stiffness is a simple and effective way of improving the realism of our model without increasing noticeably the computation time of the simulation.

In order to use the mapped cornering stiffness, the Simulink model needed data points for larger slip angles than the ones presented in [12]. There was a need to extend the graph from 20° to 45°. The points extracted from the paper, were extrapolated using a logarithmic fit function

$$F_y = -310.4ln(\alpha) + 3860.8 \quad , \tag{4.4}$$

where F_y is the lateral force and α is the slip angle.

The function was applied to the points whose angle was past the peak in force, since it provided a good fitting of the data, with a $R^2 = 0.9963$. The points used to find the fit function were the ones for slip angles from 10° to 20°.

Additionally, the Simulink model requires negative slip angles and correspondent negative forces. To accomplish this, the curve was mirrored from the first quadrant to the third quadrant.

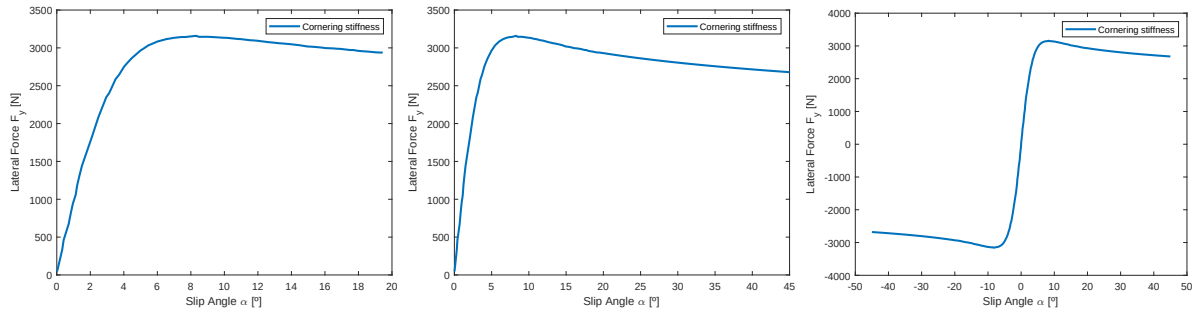

(a) Original data points [12] (b) Extended data points (c) Mirrored data points

Figure 4.2: Mapped Cornering Stiffness.

For small angles the mapped and constant corner stiffness have similar values. However, for larger angles the difference is substantial. At a slip angle of 45° the correspondent force for the mapped cornering stiffness is 2679 [N]. For the same slip angle the force for the constant cornering stiffness, 60000 [N/rad], would be 47124 [N]. Around 17 times larger and completely unrealistic. The vehicle would never be able to slip with this force.

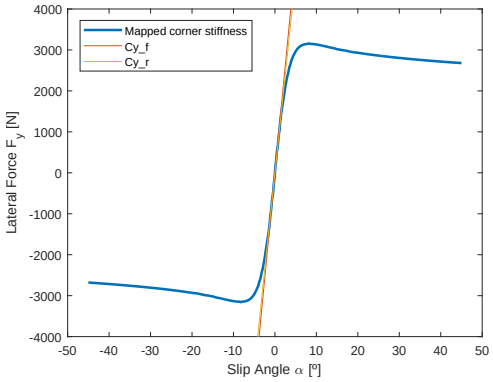

Figure 4.3: Comparison between mapped and constant cornering stiffness.

Track conditions play a significant role in tire adhesion and, consequently, in the cornering stiffness coefficients. A dry road provides considerably more friction than a wet road. Furthermore, the front wheels experience different friction levels compared to the rear wheels due to varying vertical loads and weight transfers. The experiments conducted assumed a dry road, leading to higher cornering stiffness coefficients. Table 4.1 illustrates the reduction in friction under different road conditions.

Choosing a mapped cornering stiffness over the Magic Tire Formula [18] offers several advantages, particularly in terms of computational simplicity and ease of implementation. The Magic Tire Formula, while comprehensive and highly accurate, is a complex nonlinear

Table 4.1: Cornering stiffness, acquired from an Audi S3 [13].

C_f **dry [N/rad]**	C_r **dry [N/rad]**	C_f **wet [N/rad]**	C_r **wet [N/rad]**
5.1×10^4	3.8×10^4	3×10^4	2.7×10^4

model that requires extensive parameterization and can be computationally intensive, making it challenging to use in real-time applications. Additionally, these parameters often need to be estimated, which can introduce uncertainties.

In contrast, a mapped cornering stiffness approach directly maps the stiffness coefficients to specific conditions. This method significantly reduces computational demands and simplifies implementation, providing a more straightforward and efficient way to model tire behavior under various operating conditions. Thus, the mapped approach offers a practical alternative that balances accuracy with ease of use.

4.2 PID Controller

PID controllers are used in a big range of control systems, it is a simple yet effective way of controlling a system through the tune of only 3 parameters. PID stands for Proportional, Integral and Derivative.

There are different architectures for PID controllers, parallel, series, non-standard variations, controllers without derivative part, etc. It was chosen the parallel PID architecture, Figure 4.4, because it allows us to tune the different gains and only affect the output signal. As illustrated, in the parallel architecture each one of the components applies one gain to the unaltered error input signal and it is all summed afterwards to generate the output control signal.

In a series PID, the first gain will affect the input of the second and third gain, for example. The series PID also has its uses, but it is harder to understand the effect the change of one of its gains will have, that is the reason why the parallel PID was chosen.

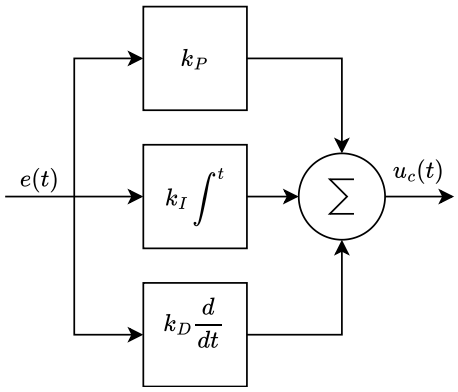

Figure 4.4: Parallel PID structure [16].

Increasing the proportional component of the controller increases the reaction speed of the system, the integral component reduces the response offset and the derivative component acts as damping, reducing oscillations [16]. The tune of the PID was made using this knowledge and through observation the response of the system. Tuning a controller is trying to find the sweet spot in terms of the response of the system. In our case the equilibrium to find was between the quality of path following, the speed of the vehicle and the reduction of oscillations. This will be shown in Section 5.3.

The time domain formula of the parallel PID is

$$u_C = k_P e(t) + k_I \int^t e(\tau)d\tau + k_D \frac{de}{dt} \quad , \tag{4.5}$$

where u_C is the ouput signal, k_P the proportional gain, k_I the integral gain, k_D the differential gain and $e(t)$ the error signal. The output of the controller is, has seen in structure, the sum of each component.

The simulations were conducted in discrete-time mode with a constant sampling period. It is acknowledged that limited sampling implies a limited bandwidth in sensors. However, the PID controller's performance is not significantly affected by the sampling frequency, this is because modern processors allow for very high sampling frequencies compared to the time constants of mechanical systems, and sensors typically provide adequate bandwidth. Thus, the discrete PID controller effectively manages the system within the constraints of discrete sampling and sensor bandwidth.

Chapter 5

Experiments and Results

In this chapter, are presented some experiments derived from João Fino's thesis work [8]. The rest of the experiments include more detailed modeling of the vehicle dynamics, including a 3DOF dual-track model and mapped cornering stiffness.

In Section 5.1 an experiment was performed to compare the single-track and dual-track 3DOF vehicle models.

In Section 5.2, using the moose test track, the yaw rate was compared between a kinematic bicycle model and the dual track 3DOF vehicle model. In this Section, the performance of the MPC controller was also evaluated for the first lane change. Different speeds were tested and a mapped cornering stiffness was firstly introduced in one of the tests.

In Section 5.3, still using the moose test track, there was the introduction of the yaw rate controller, which works together with the MPC, to improve the dynamic characteristics of the vehicle. A skeletonized version of the vehicle will be shown performing the first lane change. The results of the controllers used in tandem, will be compared to the results of just the MPC, by observing vehicle trajectory, speed, steering angle, yaw rate and yaw rate error.

5.1 Single vs Dual Track Vehicle Model

As we try to evaluate the cornering performance, the weight transfer plays a significant role in each wheel's grip. Taking this into account reveals the need to use a model which considers the forces in the four wheels.

The force applied by the wheels while cornering, is higher in the outer wheels than in

the inner wheels, due to inertia (this effect is also called weight transfer). For this reason, there was the need to go from a single-track model to a dual-track model. The single track model would only consider the forces to be applied along the longitudinal line of the CG, in this case, the inner and outer wheel would have the same vertical force applied. These assertions are supported by equation (3.1) from [17], that was presented in Section 3.2.

Single Track Vehicle Model

In Figure 5.1a are presented the results directly obtained from an experiment done by João Fino's, which consists in following the red trajectory in Figure 5.1a (left sub-figure). In this experiment it is only being used in VIENA's Car Model, the Vehicle Body 3DOF Single Track block. The Field Oriented Control (FOC) and Induction Motor are not being used for simplicity's sake. This experiment reveals that the model used is able to properly follow the trajectory and speed given, with realistic lateral acceleration values.

In Figure 5.1b the same setup was used as in Figure 5.1a but now with a different trajectory that contains a very sharp corner, in order to verify the car's behaviour in more extreme cases. As we can observe this model still presents some limitations in sharp corners, it seems like the vehicle oversteers. However, this assumption needs to be verified with more data and a different way of displaying it, but it falls out of the scope of this thesis.

Dual Track Vehicle Model

In Figure 5.1c there was a slightly different setup used, in this case I changed João Fino's Model (no Induction Motor and no FOC) to use the Vehicle Body 3DOF Dual Track model, which presented very good results in trajectory following. However, the speed profiler was not as closely followed. For the vehicle's speed, it is being used and represented, the speed of the rear left wheel. This again to simplify the experiment for now, but for the experiments performed afterwards, it was used the speed of the vehicle's center of gravity.

This test showed a very good performance in terms of trajectory following, in some parts it performed even better than the single track model. However, the speed profiler following, was not as good as previously. This will be further analysed in Section 5.2 for the moose test, using the results presented in Figure 5.5.

In Figure 5.1d the same setup was used as in Figure 5.1c but now with a different trajectory that contain a very sharp corner, in order to verify the car's behaviour in

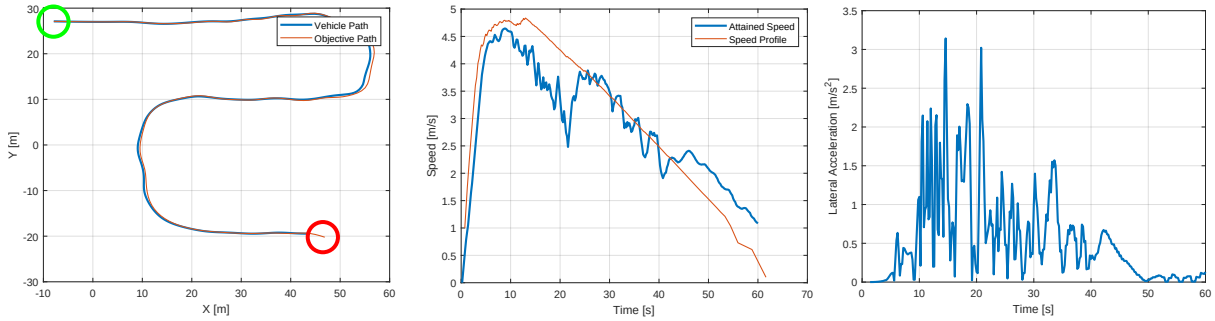

(a) **Single** track 3DOF model, Trajectory **1**

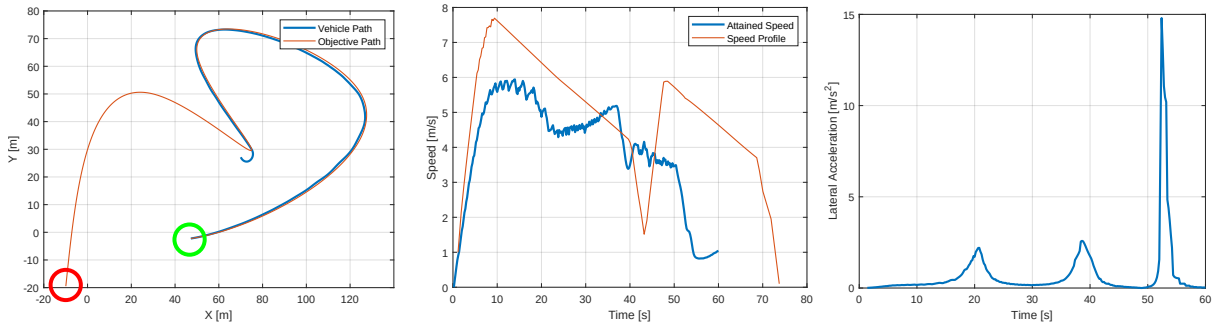

(b) **Single** track 3DOF model, Trajectory **2**

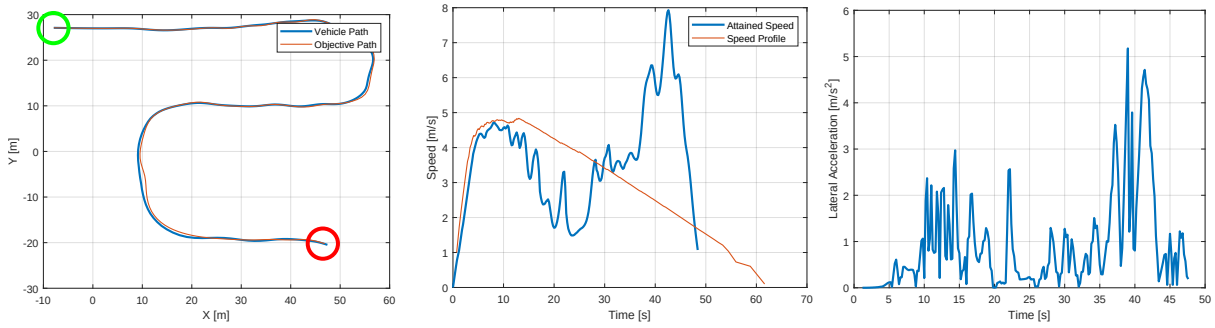

(c) **Dual** track 3DOF model, Trajectory **1**

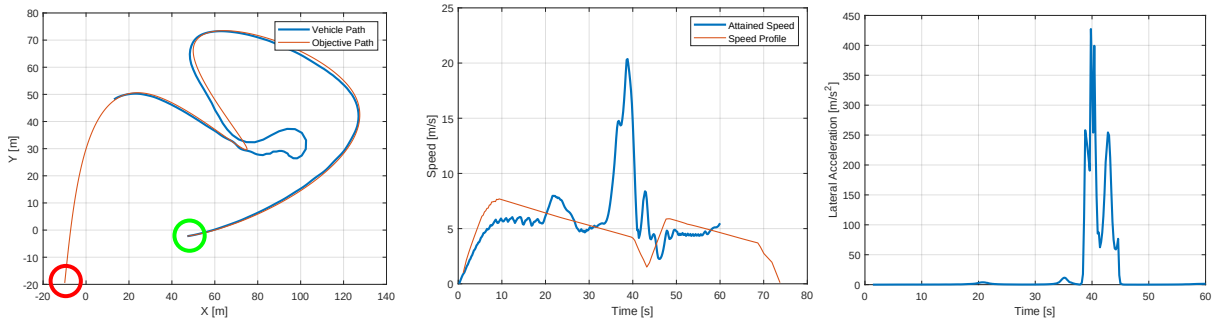

(d) **Dual** track 3DOF model, Trajectory **2**

Figure 5.1: Compare single track (a, b) vs 3DOF (c, d) vehicle models doing trajectory following using just MPC. Left column shows reference and followed trajectories. Middle column shows reference and controller computed speeds vs time. Right column shows lateral acceleration. Experiments terminated after a number of motion steps instead of detecting the end of the reference trajectory.

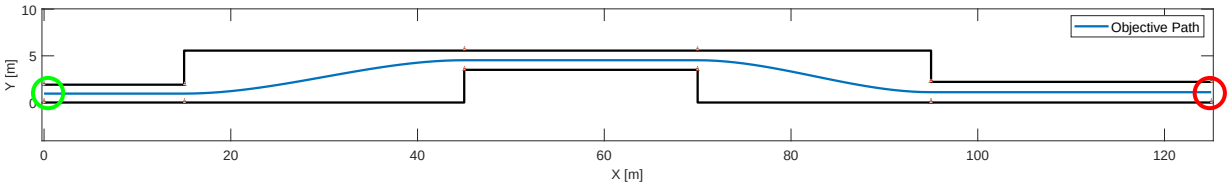

Figure 5.2: Double lane change manoeuvre test track, used in Sections 5.2 and 5.3. The reference trajectory given to the path following controller, is the blue line ("Objective Path"). The black lines represent the track limits. The vehicle starts the test at coordinates $(0, 0.95)$ and finishes at $(125, 1.1)$.

more extreme cases. As observable in Figure 5.1d (right sub-figure) the vehicle reaches impossible values of lateral acceleration, close to 430 [m/s^2] when it should be lower than 9.81 [m/s^2], so there is still a lot of work to do in order to make the simulation behave more realistically. Such high values of acceleration would only be possible in case of a collision. This problem will also be further investigated in Section 5.2, but to sum it up, it is caused by the use of a constant cornering stiffness in the 3DOF vehicle model.

The followed trajectory presented problems in the sharp corner, but this problem will not be solved in this thesis, since the decision of how the vehicle should take the tight corner is made by the MPC. The focus of this thesis is on improving the stability of the vehicle.

5.2 Yaw-Rate Studies

The tests presented in this Section were performed to create an expected yaw rate signal, which will be used afterwards by the yaw rate controller.

For these tests the cornering stiffness was initially set to a constant, but later in the Section, there was the introduction of a mapped cornering stiffness, in the vehicle model being used. The front tire cornering stiffness was set in [8] and here to $Cy\_f = 60000$ [N/rad] and the rear tire cornering stiffness set to $Cy\_r = 55000$ [N/rad].

Yaw Rate Expected vs Simulated

In the early tests there was a mistake regarding the calculation of the expected yaw rate. Instead of using l in equation (4.2) it was being used half of that value, which would correspond to l_f or l_r. This mistake resulted in having double the expected yaw rate and that was what allowed us to find it and correct it. In Figure 5.3 we can observe the effects of that mistake and infer what would be the effects of the uncertainty in vehicle

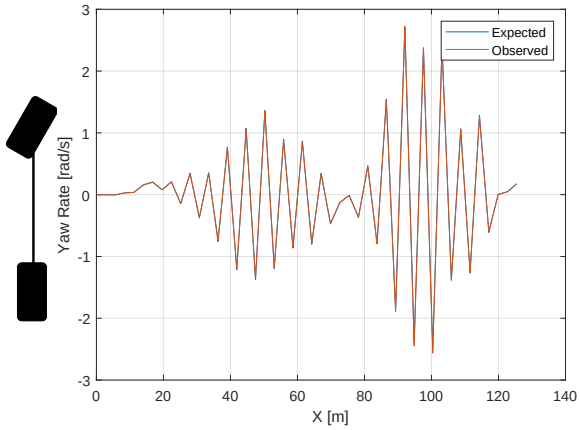

(a) Kinematic bicycle model

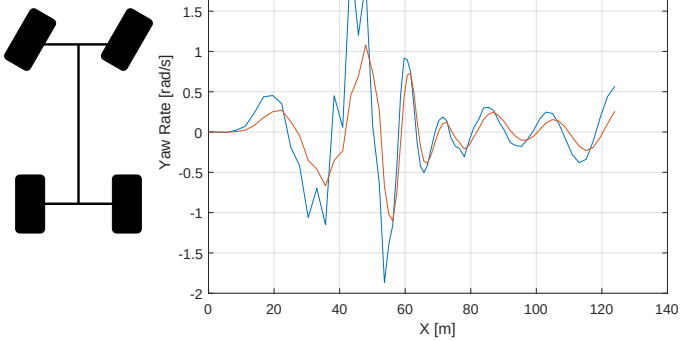

(b) 3DOF dual track vehicle model

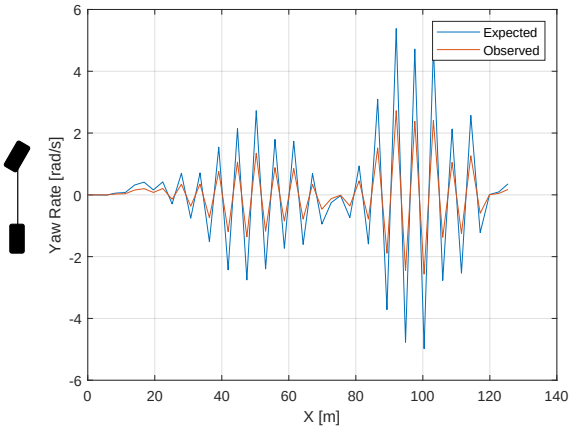

(c) Half-length kinematic bicycle model

Figure 5.3: Yaw-rate, expected vs. observed, kinematic vs. 3DOF vehicle model (a, b) and half bicycle length (c). The vehicle made one curve and counter-curve, the yaw-rate (see plots) encompasses clearly visible oscillations while the yaw angle (not plotted) approximately displays the two curves.

wheelbase. An overestimation of the vehicle wheelbase would result in an underestimation of yaw rate.

Cornering Stiffness Study

The simulations were presenting a very high deceleration on the first corner. Upon further investigation it was discarded that the MPC would be the culprit of the speed reduction, since it would happen even without the MPC controlling the acceleration. Tests were made with the MPC just controlling the steering. Since there was no problem with the longitudinal wheel force input, the other input which could be causing the problems was

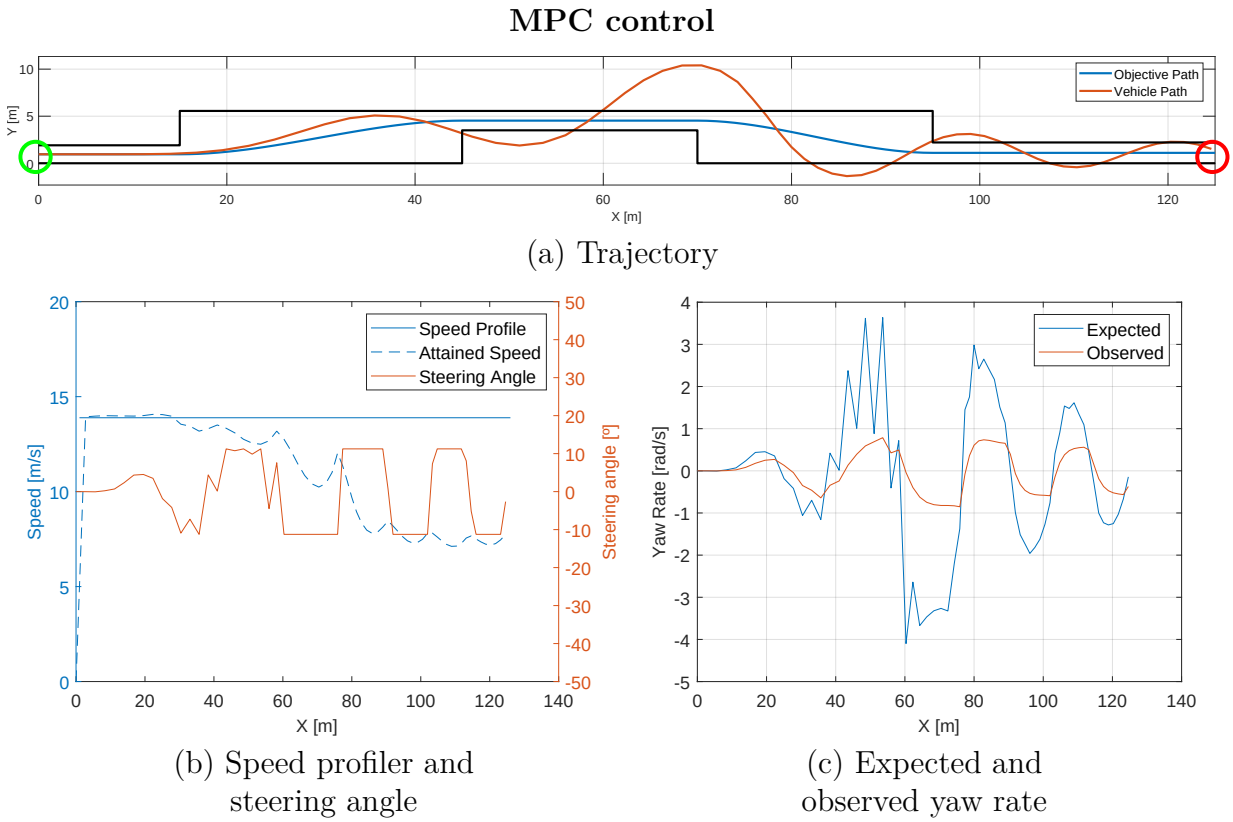

(a) Trajectory

(b) Speed profiler and steering angle

(c) Expected and observed yaw rate

Figure 5.4: MPC controlling with a steering limit of $\pi/16$ [rad]. Moose test performed at 50 [km/h]. The speed reduction is less abrupt, but the vehicle cannot follow the trajectory. The expected yaw rate is calculated based on the angle the MPC was sending the vehicle, pre-limitation. This shows that the MPC is trying to impose a higher steering angle to correct the path following error, but it is too limited to be able to correctly follow the path given.

the steering. Besides limiting the steering angle to a maximum of 45°, such a high steering angle would not be adequate for higher velocities. The front tires were having steering angles too high, effectively braking the vehicle, since the wheels would be orientated at an angle in relation to the trajectory the vehicle was following.

In order to solve the issue of unrealistic deceleration in the first curve it was tried to impose a stricter limit on the steering angle, Figure 5.4. However, this limit reduced largely the trajectory following capabilities of the vehicle. The vehicle was not capable of accurately following the trajectory.

Still not satisfied with these results, and considering the deceleration was still higher than what would be expected, it was taken a better look into the cornering stiffness. Although, the constant cornering stiffness chosen was realistic for small slip angles, for

higher slip angles (which are very important since we are trying to simulate slippage) it is largely unrealistic. The deceleration was so high because the cornering stiffness was creating an unrealistic tire force for bigger slip angles.

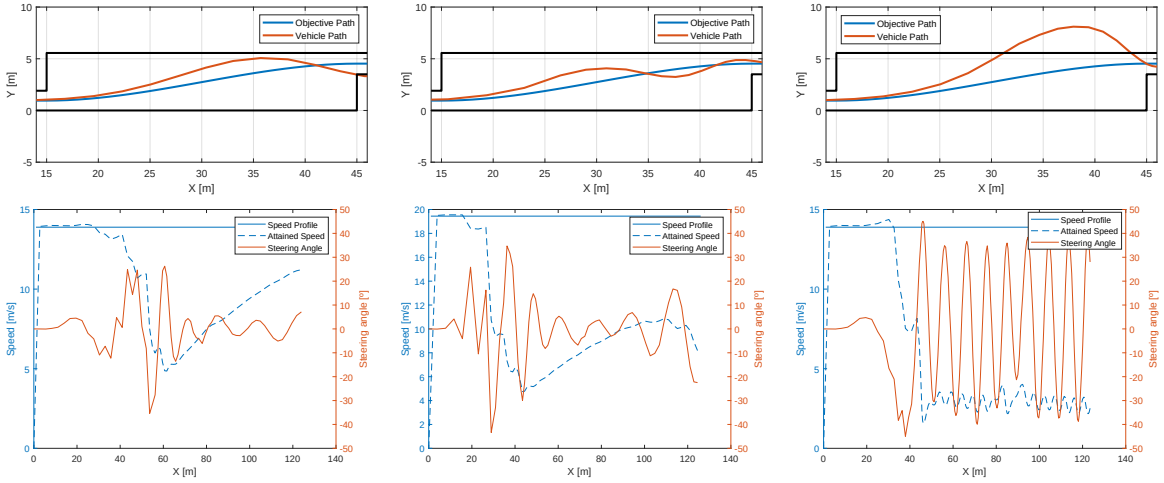

(a) **Constant** C_y 50 [km/h]

(b) Constant C_y **70** [km/h]

(c) **Mapped** C_y 50 [km/h]

Figure 5.5: Constant vs mapped cornering stiffness, moose test, using just the MPC control in all cases. Constant cornering stiffness implies some deviation from the reference path and it does show likely violation of the acceptable area for the trajectory (a). Counter-intuitive trajectory result given the higher speed values (b vs a). Mapped cornering stiffness indicates the expected significantly lower path-following accuracy (c).

Figure 5.5 shows three different experiments which allow us to evaluate the performance in the most critical part of the moose test track. It is the most challenging part due to the higher speed at which the corner is performed. It might seem that the vehicle performs better at a higher speed but in reality the vehicle which was set to the 70 [km/h], starts the corner at a lower speed because it turns the wheels more abruptly, losing speed faster.

When the speed was set to 70 [km/h] the vehicle reaches its minimum speed of 18 [km/h] at 40 [m]. When the speed was set to 50 [km/h] the vehicle reaches the same minimum speed of 18 [km/h] but much later at 60 [m], which means that it performed the first corner at a higher speed.

Figure 5.5(c) has more precise modelling of the cornering stiffness, by mapping C_y. It shows a worse trajectory following performance, which is expected since the vehicle has less grip. In these conditions the MPC alone is unable to complete the moose test

successfully and the vehicle crawls after 45 [m] because the controller is unable to raise the vehicle speed and keep it from oscillating around the reference trajectory.

5.3 MPC and Yaw-Rate Control

In this Section will be presented the results of tuning the implemented PID controller. As a way to evaluate the advantages of using the yaw rate controller, the results from the yaw rate controller will be compared to the results of using just the MPC. This way we can assess the need of an yaw rate controller, which might complement the MPC and generate better results. By revealing the need to use a better controller or one that is better tuned, this will lead improvements in the handling capabilities of the vehicle. These tests will show the need of changing and improving the previously implemented controller.

Tunning Accounting Cornering Stiffness

In order to mitigate the issue of unrealistic deceleration in the first curve another strategy was also followed, the tune of the controller would be done so it would minimize the speed loss while cornering, Figure 5.6. Keeping a reasonable speed is important in this kind of test, in a real scenario, when the vehicle changes lane it is going against the oncoming traffic. So we should try to perform the manoeuvre as fast as possible.

Figure 5.7 shows a 2D model of the vehicle while performing the moose test, with a controller composed of MPC and yaw rate controller. In this representation it is possible to observe the wheels steering to compensate for the vehicle getting away from the given trajectory. The controllers used, allowed for a successful completion of the task and a good behaviour of the vehicle in the hardest part of the track. The vehicle passes between the gates formed by the cones and between them it stays inside the black line, which represents the track limits. It is also possible to observe the deceleration of the vehicle after it turns the wheels sharply.

Using the mapped cornering stiffness we are reducing drastically the amount of grip between the tires and the road. Expectedly, this worsens the performance of the simulated vehicle in comparison to the linear cornering stiffness tests. The vehicle has some difficulty following the path given at a higher speed and is only able to accurately follow the path after it decelerates. We will be able to see in Figure 5.8, that the vehicle is getting away from the ideal trajectory. This results from the MPC being used at higher speeds and in a vehicle model which it was not tuned for. Using the yaw rate controller with the MPC,

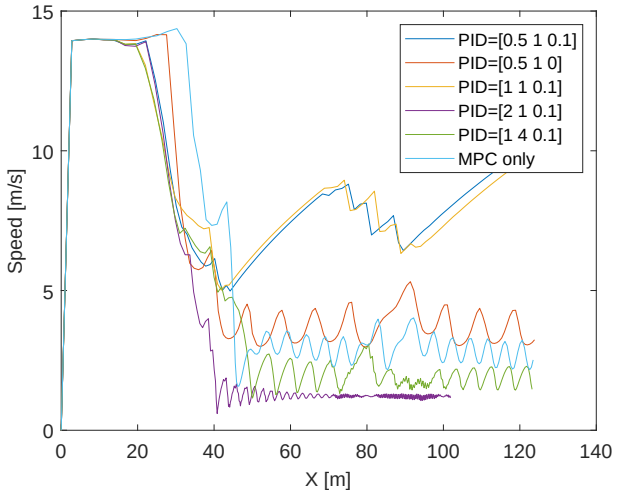

Figure 5.6: Speed reduction comparison while cornering. MPC compared with the MPC and yaw rate controller, tuned with different PID values. Moose test performed at 50 [km/h] using the mapped cornering stiffness. PID = [0.5 1 0.1] was the best tune found, for the combination of low speed reduction (relatively), improved stability and good path following. Considering the MPC alone as the baseline, the speed characteristics were greatly improved with the new controller (MPC and yaw rate control).

besides improving vehicle stability, it also decreases the distance between the vehicle's path and the ideal path.

Comparison MPC vs MPC and Yaw-Rate Control

The results obtained in this Section are for the mapped cornering stiffness. An equal cornering stiffness was applied to the front and rear tires.

There were other tests with different PID gains which yielded similar results. However, these gains were chosen by using the following criteria: Least speed reduction, stability of the path following and smoothness of yaw rate. The last criterion was chosen in order to not have a vehicle which follows well the trajectory but would be terribly uncomfortable for its passengers due to the over-reactivity of the steering system.

After testing what the yaw rate controller was capable of doing, it was important to observe the performance of the MPC controller applied to a more realistic and complex model, Figure 5.8, composed of the 3DOF vehicle model and the mapped cornering stiffness.

This test results reveal the problems of tuning a MPC with a kinematic model. Due to the lack of realism of the kinematic model, when the MPC is used in a more realistic model it fails in ways unaccounted for. For example in this case, probably due to the

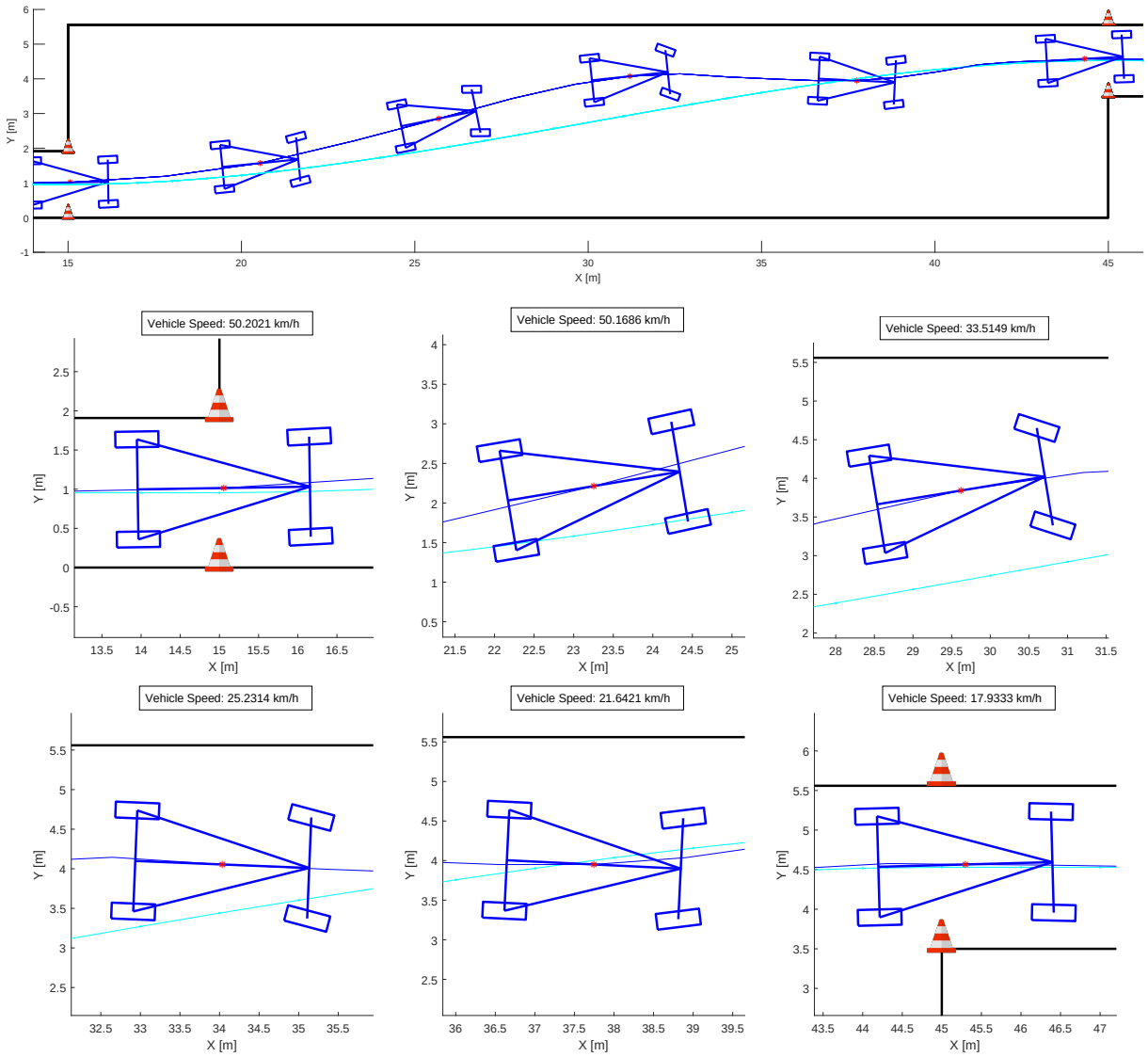

Figure 5.7: Moose test, 2D vehicle representation. Test performed with MPC and yaw rate control. The vehicle goes through both gates successfully, besides getting away from the given reference trajectory (cyan blue), it stays within the allowed limits. There is a speed reduction resultant from the losses while steering.

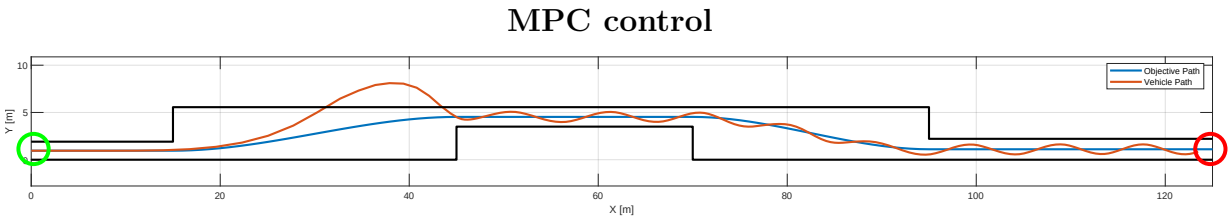

(a) Trajectory

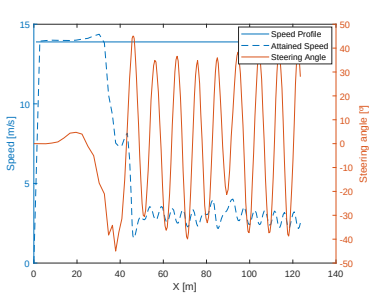

(b) Speed profiler and steering angle

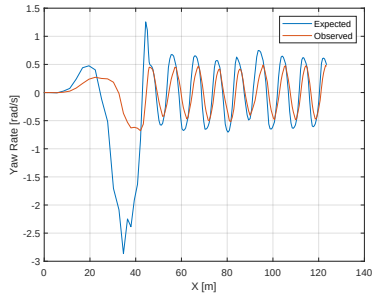

(c) Expected and observed yaw rate

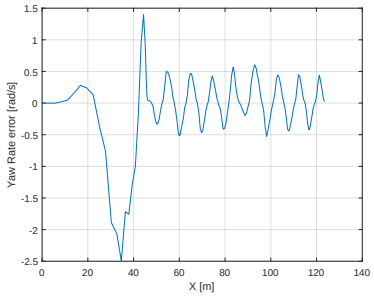

(d) Yaw rate error

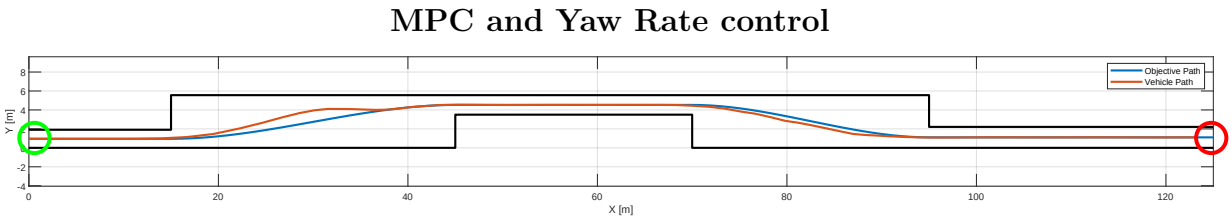

(e) Trajectory

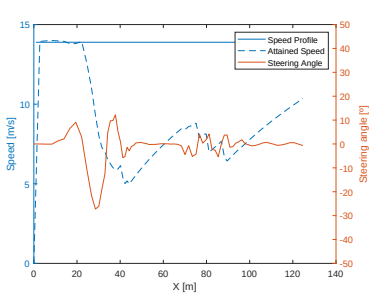

(f) Speed profiler and steering angle

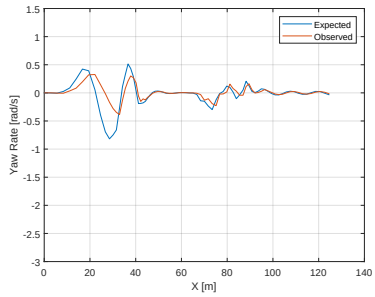

(g) Expected and observed yaw rate

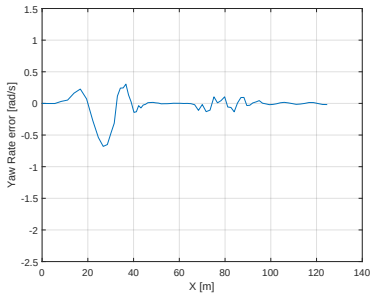

(h) Yaw rate error

Figure 5.8: Yaw Rate control with *non constant stiffness*, i.e. added *mapped cornering stiffness*. Moose test performed at 50 [km/h]. The MPC stops accelerating in the corners and it speeds up while on a straight line. As the MPC alone cannot follow the trajectory without oscillating, the speed is drastically reduced. MPC and yaw rate control together follows the trajectory smoothly at a much higher speed.

inertia of the vehicle and the nonlinearity of the force applied by the tires, the vehicle oscillates around the reference trajectory, while performing the test at a much lower speed than the new controller. It is by taking the controller out of its comfort zone that we can truly test it and then with those results build a more robust controller.

These results also illustrate the problems that could arise from applying the MPC controller tuned for a kinematic model, to the real VIENA. For the previous implementations and at lower speeds this controller showed a good performance. However, challenging the controller demonstrates that there is still a long way to go in order to have a capable VIENA controller, which is capable of performing in different scenarios. A passenger vehicle with the characteristics of VIENA should be able to follow a pre-planned trajectory or react quickly to an obstacle at low speeds but also at higher speeds and the new yaw rate controller, although having a big way to still go to be used it takes VIENA closer to that objective.

Chapter 6

Conclusions and Future Work

The thesis proposes the implementation of an Electronic Stability Controller (ESC) in the VIENA project, aimed at enhancing vehicle safety. This project will serve as a crucial platform to educate new engineers at Instituto Superior Técnico, ensuring that they are better qualified to work in autonomous electric vehicles.

The main technical constraint identified in this work was the lack of an ABS system in the Fiat Seicento Electra, which would provide a way of actuating autonomously and individually the brakes of the vehicle and would also provide a set of needed sensors, such as the wheel speed sensors. Due to this limitation, the thesis focus shifted toward an alternative solution, a steering-based yaw rate controller. This type of controller is not commonly used in production vehicles but holds potential with advancements in technology, such as autonomous vehicles and steer-by-wire systems. The studies on vehicle dynamics and ESC enabled more realistic simulations using the implemented controller.

Our initial experiments focused on testing the path-following controller while transitioning from the previous VIENA model, a 3DOF single track model, to a 3DOF dual track model. Although we are still in the process of building the systems and have not yet deployed them in real vehicles, we are making significant progress. The results we are obtaining in various aspects are encouraging and indicate that we are getting closer to real-world applications.

Our simulations and preliminary tests suggest improvements in stability and accuracy, reinforcing our confidence in the potential of our developed models. However, the outcomes related to speed and lateral acceleration suggested that the model required tuning to exhibit a more realistic behavior. One necessary adjustment was the introduction of mapped cornering stiffness. The original model utilized a constant cornering stiffness,

a straightforward approach for vehicle modeling, but insufficiently realistic for considering wheel slippage. This modeling approach generated forces that increased significantly with the slip angle, an unrealistic scenario where increased friction forces would occur on a slippery road solely due to larger steering angles. The mapped cornering stiffness enables the modeling of lateral (friction) force with an upper bound when encountering large slip angles.

The implementation of a functional yet simple yaw rate controller significantly improved the vehicle's stability performance. Consequently, the trajectory-following performance also increased substantially. A more stable vehicle can better follow the received inputs without running off track. Much of the work involved tuning the controller, balancing the maintenance of exit speed, trajectory quality, and reduction of oscillations.

For future work, there are various opportunities to improve the implemented system. This system can be integrated with a regular ESC, as controlling both steering and brakes should yield even better results. Additionally, improvements can be made to the steering-based ESC by considering other control variables, such as lateral acceleration, wheel speed, and motor torque. Integration with a regular ESC would allow the control of more variables, such as the braking pressure in each wheel and motor acceleration.

Bibliography

[1] ISO 3888-1. Passenger cars - test track for a severe lane-change manoeuvre. *Part 1: Double lane-change*, Dec 2018.

[2] Tim Beissmann. Infiniti Q50: world-first steer-by-wire technology detailed. `https://www.drive.com.au/news/infiniti-q50-world-first-steer-by-wire-technology-detailed/`. Accessed on 26/05/2024.

[3] Bert Breuer and Karlheinz Bill. *Bremsenhandbuch: Grundlagen, Komponenten, Systeme, Fahrdynamik*. Vieweg, Wiesbaden, 2006.

[4] Chih-Keng Chen, Trung-Kien Dao, and Min-Fang Lo. A compensated-yaw-moment-based vehicle stability controller. In *2008 Chinese Control and Decision Conference*, pages 892–897, 2008.

[5] Johannes Deichmann, Eike Ebel, Kersten Heineke, Ruth Heuss, Martin Kellner, and Fabian Steiner. Autonomous driving's future: Convenient and connected. `https://www.mckinsey.com/industries/automotive-and-assembly/our-insights/autonomous-drivings-future-convenient-and-connected#/`, Jan 2023. Accessed on 07/06/2023.

[6] Francisco Durão Leitão Enguita. Stereo-camera calibration auto-tuning for simultaneous localization and mapping. Master's thesis, Instituto Superior Técnico, University of Lisbon, Portugal, 2023.

[7] Susan Ferguson. The effectiveness of electronic stability control in reducing real-world crashes: A literature review. *Traffic injury prevention*, 8:329–38, Jan 2008.

[8] João Pedro Gonçalves Pascoal Duarte Fino. Path following for autonomous electric vehicles. Master's thesis, Instituto Superior Técnico, University of Lisbon, Portugal, 2023.

[9] Thomas D. Gillespie. *Fundamentals of Vehicle Dynamics*. SAE International, Warrendale, 1992.

[10] Nidhi Kalra and Susan M. Paddock. Driving to safety: How many miles of driving would it take to demonstrate autonomous vehicle reliability? *Transportation Research Part A: Policy and Practice*, 94:182–193, 2016.

[11] Tim Kaufmann, Scott Millsap, Brian Murray, and Jim Petrowski. Development experience with steer-by-wire. In *SAE Technical Paper*, Aug 2001.

[12] Junho Lee and Hyuk Jun Chang. Analysis of explicit model predictive control for path-following control. *PLoS ONE*, 13, Mar 2018.

[13] Christian Lundquist and Thomas B. Schön. Recursive identification of cornering stiffness parameters for an enhanced single track model. *IFAC Proceedings Volumes*, 42:1726–1731, Apr 2009.

[14] MathWorks. 3DOF rigid vehicle body to calculate longitudinal, lateral, and yaw motion - Simulink. `https://www.mathworks.com/help/vdynblks/ref/vehiclebody3dof.html`. Accessed on 23/05/2023.

[15] MathWorks. Piecewise Cubic Hermite Interpolating Polynomial (PCHIP) - MATLAB. `https://www.mathworks.com/help/matlab/ref/pchip.html#bvjbz1m-2`. Accessed on 23/05/2024.

[16] Mohammad Hassan Moradi, Michael A. Johnson, and James Crowe. *PID control: New Identification and Design Methods*. Springer-Verlag, London, 2005.

[17] Andrzej G Nalecz and Alan C Bindemann. Handling properties of four wheel steering vehicles. *SAE transactions*, pages 63–82, 1989.

[18] Hans B Pacejka and Egbert Bakker. The magic formula tyre model. *Vehicle system dynamics*, 21(S1):1–18, 1992.

[19] Brian Paden, Michal Čáp, Sze Zheng Yong, Dmitry Yershov, and Emilio Frazzoli. A survey of motion planning and control techniques for self-driving urban vehicles. *IEEE Transactions on Intelligent Vehicles*, 1(1):33–55, 2016.

[20] Filipe Parrado. Steering and speed control for autonomous electric vehicles. Master's thesis, Instituto Superior Técnico, University of Lisbon, Portugal, 2021.

[21] Fábio Portelinha. Steering and speed control for autonomous electric vehicles. Master's thesis, Instituto Superior Técnico, University of Lisbon, Portugal, 2022.

[22] Pratik. Anti-lock braking system/abs: Working, diagram, principle, with pdf. `https://mechcontent.com/antilock-braking-system-pdf/`, Apr 2023. Accessed on 19/05/2023.

[23] C.A. Rabbath and D. Corriveau. A comparison of piecewise cubic hermite interpolating polynomials, cubic splines and piecewise linear functions for the approximation of projectile aerodynamics. *Defence Technology*, 15:741–757, Oct 2019.

[24] Rajesh Rajamani. *Vehicle Dynamics and control*. Springer, New York, 2012.

[25] Adnan Shaout and Kevin Mcgirr. Real-time systems in automotive applications: Vehicle stability control. *Electrical Engineering Research Vol. 1 Iss. 4*, Oct 2013.

[26] Luqi Tang, Fuwu Yan, Bin Zou, Kewei Wang, and Chen Lv. An improved kinematic model predictive control for high-speed path tracking of autonomous vehicles. *IEEE Access*, 8:51400–51413, 2020.

[27] Takumi Ueno, Binh Minh Nguyen, and Hiroshi Fujimoto. Direct yaw moment control for electric vehicles with variable-rate-slip-ratio-limiter based driving force control. In *Proceedings - 2023 IEEE International Conference on Mechatronics, ICM 2023*. Institute of Electrical and Electronics Engineers Inc., 2023.

[28] João Pedro Lino Vargas. Three-wheeled vehicle modeling with multibody suspension implementation. Master's thesis, Instituto Superior Técnico, University of Lisbon, Portugal, 2022.

[29] Johan Wahlström, Isaac Skog, and Peter Händel. Detection of dangerous cornering in gnss-data-driven insurance telematics. *IEEE Transactions on Intelligent Transportation Systems*, 16(6):3073–3083, 2015.

[30] Jake Weaver. Lexus RZ 450e: your questions answered. `https://mag.lexus.co.uk/lexus-rz/`. Accessed on 26/05/2024.

[31] The World Health Organization (WHO). Global status report on road safety 2018. https://www.who.int/publications/i/item/9789241565684, 2018. Accessed on 08/06/2023.

[32] Kevin Williams. Huzzah, The Tesla Cybertruck Has Steer-By-Wire. https://insideevs.com/news/698794/tesla-cybertruck-steer-wire/. Accessed on 26/05/2024.

[33] Fitri Yakub and Yasuchika Mori. Comparative study of autonomous path-following vehicle control via model predictive control and linear quadratic control. *Proceedings of the Institution of Mechanical Engineers, Part D: Journal of Automobile Engineering*, 229:1695–1714, Oct 2015.

[34] Li Zhai, Tianmin Sun, and Jie Wang. Electronic stability control based on motor driving and braking torque distribution for a four in-wheel motor drive electric vehicle. *IEEE Transactions on Vehicular Technology*, 65(6):4726–4739, 2016.